Atmos. Meas. Tech. Discuss., 7, 12873–12927, 2014
www.atmos-meas-tech-discuss.net/7/12873/2014/
doi:10.5194/amtd-7-12873-2014

Atmospheric Measurement Techniques Discussions

On the microwave optical properties of randomly oriented ice hydrometeors

P. Eriksson[1], **M. Jamali**[1], **J. Mendrok**[2], **and S. A. Buehler**[3]

[1]Earth and Space Sciences, Chalmers University of Technology, 41296 Gothenburg, Sweden
[2]Division of Space Technology, Lulea University of Technology, 98128 Kiruna, Sweden
[3]Meteorological Institute, Center for Earth System Research and Sustainability, University of Hamburg, Bundesstrasse 55, 20146 Hamburg, Germany

Received: 2 December 2014 – Accepted: 3 December 2014 – Published: 21 December 2014

Correspondence to: P. Eriksson (patrick.eriksson@chalmers.se)

Published by Copernicus Publications on behalf of the European Geosciences Union.

Abstract

Microwave remote sensing is important for observing the mass of ice hydrometeors. One of the main error sources of microwave ice mass retrievals is that approximations around the shape of the particles are unavoidable. One common approach to represent particles of irregular shape is the soft particle approximation (SPA). We show that it is possible to define a SPA that mimics mean optical particles of available reference data over narrow frequency ranges, considering a single observation technique at the time, but SPA does not work in a broader context. Most critically, the required air fraction varies with frequency and application, as well as with particle size. In addition, the air fraction matching established density parameterisations results in far too soft particles, at least for frequencies above 90 GHz. That is, alternatives to SPA must be found.

One alternative was recently presented by Geer and Baordo (2014). They used a sub-set of the same reference data and simply selected as "shape model" the particle type giving the best overall agreement with observations. We present a way to perform the same selection of a representative particle shape, but without involving assumptions on particle size distribution and actual ice mass contents. Only an assumption on the occurrence frequency of different particle shapes is still required. Our analysis leads to the same selection of representative shape as found by Geer and Baordo (2014). In addition, we show that the selected particle shape has the desired properties also at higher frequencies as well as for radar applications.

Finally, we demonstrate that in this context the assumption on particle shape is likely less critical when using mass equivalent diameter to characterise particle size, compared to using maximum dimension, but a better understanding of the variability of size distributions is required to fully characterise the advantage.

Further advancements on these subjects are presently difficult to achieve due to a lack of reference data. One main problem is that most available databases of pre-calculated optical properties assume completely random particle orientation, while for certain conditions a horizontal alignment is expected. In addition, the only database

AMTD
7, 12873–12927, 2014

covering frequencies above 340 GHz has a poor representation of absorption as it is based on outdated refractive index data, as well as only covering particles having a maximum dimension below 2 mm and a single temperature.

1 Introduction

Microwave techniques are gaining in importance for satellite observations of hydrometeors, i.e. clouds and precipitation. The main measurement target of microwave sensors is mass content estimates, possibly in the form of a precipitation rate. The detection mechanism used (absorption or scattering) depends on phase (liquid, ice or mixed), frequency, and on whether the instrument is active or passive. For example, for non-precipitating liquid droplets passive measurements rely on absorption, while radars rely on back-scattering. The signature of ice hydrometeors in passive data is a mix of scattering and absorption features, where in general the scattering part dominates (Sect. 4).

The accuracy of the retrievals depends on technique applied and a number of variables, including observational noise and limitations in the radiative transfer code used. However, the main retrieval error sources are frequently uncertainties associated with the microphysical state of the particles, i.e. phase, size, shape and orientation. This study focuses on the impact of assumed shape, that is probably the microphysical quantity with least hope of being retrievable based on microwave data alone. Information on particle size can be obtained by combining data from different frequencies (Evans and Stephens, 1995a; Buehler et al., 2007; Jiménez et al., 2007), while the phase of the particles is largely determined by the atmospheric temperature. Measuring horizontal and vertical polarisation simultaneously reveals if the particles have a tendency to horizontal alignment or if their orientation is completely random (e.g. Hall et al., 1984; Hogan et al., 2003; Davis et al., 2005; Eriksson et al., 2011b).

Shape is normally not a critical aspect for purely liquid particles, as they are throughout quasi-spherical. The deviation from a strict spherical shape increases with droplet

AMTD
7, 12873–12927, 2014

size and fall speed. On the other hand, the shape of frozen hydrometeors is highly variable, both as single crystals (needles, plates, columns, rosettes, dendrites, etc.) and as aggregates (see reviews by Heymsfield and McFarquhar, 2002; Baran et al., 2011). The shape is frequently denoted as the habit. It is unlikely that the air volume sampled contains a single ice particle shape, i.e. a habit mix can be expected. Furthermore, this mix normally varies with particle size. In principle, the shape of each particle should be known to avoid a related retrieval error, but this is not a feasible goal. Instead some "shape model" must be applied and the main aim of this study is to examine such models for microwave sounding of pure ice hydrometeors.

Considering the ice particles to be solid spheres is probably still the main microwave shape model. This approach is for example used in the standard 2B-CWC-O CloudSat retrievals by Austin et al. (2009). It is also applied in e.g. the Community Radiative Transfer Model (CRTM, Liu et al., 2013). Accordingly, retrieval systems (e.g. Boukabara et al., 2013; Gong and Wu, 2014) and radiance assimilation based on CRTM inherit the assumption of solid spheres. Furthermore, this particle type has throughout been assumed in cloud ice retrievals based on limb sounding data (Wu et al., 2008; Rydberg et al., 2009; Millán et al., 2013). A main reason for the popularity of this shape model is that the single scattering properties are simply calculated by well-established Mie codes.

Another common model is the "soft particle approximation" (SPA) where the particles are treated to consist of a homogeneous mix of ice and air. This approach requires that the volume or mass fraction of air and the corresponding refractive index of the ice-air mix are determined, see Sects. 2 and 5. SPA could in principle be used with a range of simplified particle forms, but it seems that only spheres and spheroids have been used so far. Spheroids are not treated by Mie theory, but are covered by the also computationally efficient T-matrix method (Mishchenko et al., 1996). One application of SPA for practical retrievals is Zhao and Weng (2002). A more recent example is Hogan et al. (2012), arguing for using a soft spheroid model for cloud radar inversions. In addition, SPA has widely been used in studies to mimic measured radiances by

AMTD
7, 12873–12927, 2014

radiative transfer tests (e.g. Bennartz and Petty, 2001; Skofronick-Jackson et al., 2002; Doherty et al., 2007; Meirold-Mautner et al., 2007; Kulie et al., 2010) where the air fraction is either set to be fixed or derived from some parametric relationship between particle size and effective density.

Single scattering properties for arbitrary particle shapes can be calculated by e.g. the Discrete Dipole Approximation (DDA, Draine and Flatau, 1994). For example, DDA is used for incorporating realistic particle shapes in the retrievals presented by Evans et al. (2012). This study is likely the most ambitious microwave retrieval set-up with regards to particle shape, but it deals only with a specific measurement campaign and it does not provide any general conclusions. Publicly available databases of DDA results for common particle shapes are reviewed in Sect. 3. These databases were used by Kulie et al. (2010) to test if simulations could recreate some collocated radar and passive microwave data when applying different particle shapes. In a similar study by Geer and Baordo (2014) only passive data were considered but a more wide set of frequencies and atmospheric conditions were investigated. They found that a sector-like snowflake model gave the smallest overall error for the simulations performed. This choice will replace a SPA treatment as the default for the snow hydrometeor category in the RTTOV-SCATT (Bauer et al., 2006) package (Geer and Baordo, 2014). In Sect. 6 an alternative version of the approach of Geer and Baordo (2014) is tested, that does not involve any assumption on PSD or actual ice masses.

DDA calculations have also been used in a more direct manner to investigate shape aspects. For example, Kim (2006) compared DDA and solid sphere results and claimed that particle shape is less critical for size parameters below 2.5 (see Eq. 2 for the definition), but only a few DDA shapes and frequencies were considered, radar back-scattering was ignored, and no quantitative error estimate was given. Comparisons between DDA and corresponding SPA data are found in e.g. Liu (2008); Nowell et al. (2013) and Liao et al. (2013), but the results have throughout a limited scope and we have found no comprehensive analysis of the limitations of SPA. An important result was obtained by Liu (2004), showing that an optimal "softness parameter", to be ap-

AMTD
7, 12873–12927, 2014

plied in a SPA framework, varies with frequency. The same conclusion has also been reached in indirect ways by others, as pointed out by Geer and Baordo (2014).

From the perspective of mass retrievals it is most practical to characterise the size of the particles through their equivalent mass ice sphere diameter, d_e:

$$d_e = \sqrt[3]{\frac{6m}{\rho_i \pi}}, \quad (1)$$

where m is the particle mass and ρ_i is the density of (solid) ice. We define the size parameter, x, correspondingly:

$$x = \frac{\pi d_e}{\lambda}, \quad (2)$$

where λ is the wavelength at which the measurement is performed.

In microwave sounding, the mass is inferred from estimated extinction or backscattering coefficients. Any type of such coefficient, γ, can be expressed as

$$\gamma = \int_0^\infty N(d_e)\overline{\sigma_\gamma}(d_e)\,\mathrm{d}d_e, \quad (3)$$

where $N(d_e)$ is the particle size distribution (PSD) and $\overline{\sigma_\gamma}(d_e)$ is the local average cross-section for particles having a mass matching d_e. In its turn, Eq. (3) implies that trying to estimate $\overline{\sigma_\gamma}(d_e)$ from observed satellite data (as done in e.g. by Kulie et al., 2010; Geer and Baordo, 2014) requires a good knowledge of both the mass of frozen hydrometeors and the PSD.

Another common way to express particle size is by the maximum diameter, d_m. We start the study by using d_e, because usage of d_m demands that the relation between d_m and particle mass must be introduced. Such relationships depend on particle shape, and for the basic purpose of this study that is a problematic complication. By using d_e,

AMTD
7, 12873–12927, 2014

particle shape only influences $\overline{\sigma_\gamma}(d_e)$. However, as d_m is probably more frequently used than d_e, this alternative to characterise particle sizes is considered as last step of the study (Sect. 7).

In summary, our scope is the approximation of particle shape in microwave retrievals of the mass of pure ice hydrometeors. Focus is put on SPA and the basic conclusion of Geer and Baordo (2014). Both passive and active measurements are considered as merging information from different sensor types is already a fact (e.g. Rydberg et al., 2009; Kulie et al., 2010), and such synergies should in the future just grow in importance. The practical aim can be seen as finding a shape model that gives a good estimate of $\overline{\sigma_\gamma}(d_e)$, for relevant optical properties, over a large range of particle sizes, frequencies, measurement techniques and possible habit mixes. Existing DDA data are reviewed and used as reference. Only complete random orientation is treated because most established publicly available DDA databases are currently limited to this assumption on orientation.

Further, compared to earlier similar works, much higher attention is given to frequencies above 200 GHz. Ice mass retrievals are already performed at sub-millimetre wavelengths using limb sounding (Wu et al., 2008; Rydberg et al., 2009; Millán et al., 2013) and airborne sensors (Evans et al., 2012). Additionally, a strong motivation for this assessment are upcoming sub-millimetre instruments: the European ISMAR (International SubMillimetre Airborne Radiometer) airborne instrument and the ICI (Ice Cloud Imager) sensor to be part of the next series of Metop satellites. ICI is a down-looking sub-millimetre cloud ice sensor, a concept that has already been described in several articles (Evans and Stephens, 1995a; Buehler et al., 2007, 2012), but for which so far no actual satellite sensor has been available. This study is part of our overall effort to build the scientific foundation for the analysis of first the ISMAR airborne and then eventually the ICI satellite data.

AMTD
7, 12873–12927, 2014

2 Refractive index

Any calculation of single scattering properties, i.e. independently if Mie, T-matrix or DDA calculations are performed, requires that the refractive index is specified. Parameterisations and expressions related to the refractive index of ice at microwave frequencies are reviewed in this section. Both the real (n') and imaginary (n'') part of the complex refractive index n are relevant. Some relationships are more easily expressed in terms of the (relative, complex) dielectric constant, ϵ. Neglecting magnetic effects, which is a good assumption here, this quantity is related to the (complex) refractive index as:

$$n = \sqrt{\epsilon} \tag{4}$$

2.1 Pure ice models

Providing complex refractive index practically over the complete electromagnetic spectrum in the form of data tables, Warren (1984), in the following referred to as W84, has been a long-term standard in atmospheric science for the refractive index of pure water ice. Hufford (1991, H91) developed a parameterisation for microwave frequencies up to 1 THz based on Debye and Lorenz theories with parameters fitted from measured data. The parameterisation was incorporated in the MPM93 atmospheric propagation model by Liebe et al. (1993). Compared to W84, H91 generally predicts lower n'' for frequencies < 350 GHz (see Fig. 1, right panel). Consistent with measurements it predicts a stronger increase of n'' with temperature than W84 at sub-millimetre frequencies.

In the advent of sub-millimetre observation techniques, Jiang and Wu (2004, J04) added a higher order frequency term, as suggested by Mishima et al. (1983), to H91 in order to cover frequencies up to 3 THz. Resulting n'' agree well with H91 till about 1 THz as shown in Fig. 1. Beyond 1 THz, where H91 claims no validity, J04's n'' exhibits the frequency and temperature dependence pattern expected from measured far-infrared behaviour of n''. Zhang et al. (2001, Z01) did the first measurements of both n' and n'' at sub-millimetre frequencies and atmospheric temperatures. For n'' they found a linear temperature dependence of about 1 % K^{-1}. The measurements agree quite well with

AMTD
7, 12873–12927, 2014

the H91 and J04 models. However, the Z01 model falls short of reproducing their own measurements – it predicts very low values over all frequencies (see Fig. 1) and all temperatures.

Mätzler et al. (2006, M06) introduced a permittivity parameterisation that consolidates most earlier models and measurements. Regarding imaginary part, it agrees well with the J04 model, particularly at microwave frequencies, deviating at maximum by 5 % at higher frequencies and high temperatures. The largely revised and updated version of W84, the Warren and Brandt (2008, W08) data, incorporates the M06 model at $T = -7\,^{\circ}\mathrm{C}$ and proposes M06 as the model of choice at wavelengths beyond 200 µm when temperature dependence should be considered.

J04 found their model to be within 12 % of the imaginary permittivity measurements for frequencies below 800 GHz, and within 15–40 % above 800 GHz. M06 estimated the uncertainty of their model from the SDs of measurements to 5 % at 270 K and 14 % at 200 K. W08 state the uncertainty of their n'' data to be 10 % ($T = -7\,^{\circ}\mathrm{C}$). Compared to recent models, the once quasi-standard model W84 strongly overestimates n'' at millimetre wavelengths (up to a factor of 5), underestimates it at sub-millimetre wavelengths (up to a factor of 2) and overestimates it in the far-infrared (up to a factor of 2).

In contrast to n'', n' is generally considered to be known with higher accuracy and to vary little to negligibly with both temperature and frequency. The measurements by Z01 confirm the small frequency dependence (0.3 % over 250–1000 GHz) and do not show significant temperature dependence. The different models mentioned above provide slightly different relations of n' with frequency and temperature. However, we find refractivity ($n' - 1$) from all models to agree with M06 within 1.3 %, according to the left panel of Fig. 1. Based on estimates on propagation of n' uncertainty to optical properties, we conclude that the uncertainty in n' is not a limiting factor and choice of model is not critical.

In summary, M06 seems the best choice for microwave to far-infrared imaginary refractive index data. In view of the effects that errors in imaginary refractive index

AMTD
7, 12873–12927, 2014

have on cloud optical properties, we strongly suggest to no longer use the Warren (1984) data in future.

2.2 Mixing rules

The parameterisations reviewed above deal with solid ice, while in the soft particle approximation (Sect. 5) the particles are treated to consist of a homogeneous mixture of ice and air. The standard procedure to assign a refractive index to the mixture is by applying a so called mixing rule. In this paper we compare some commonly used mixing rules from a purely practical perspective, a more theoretical review of mixing rules is provided by Sihvola (2000).

Throughout, we will assume the refractive index of air to be $1 + i0$, in other words we assume that the optical properties of air are like those of vacuum. Of course, for the radiative transfer problem as a whole both absorption and refraction by air matter strongly. But given the much larger refractive index of ice we neglect this in the calculation of the single scattering properties, as commonly done also by other authors.

Three mixing rules are considered: "Maxwell–Garnett" (Garnett, 1906), "Bruggeman" (Bruggeman, 1935) and "Debye" (Debye, 1929). All these formulas operate with dielectric constants. The Debye mixing rule is

$$\frac{\epsilon_e - 1}{\epsilon_e + 2} = \frac{f_1^v(\epsilon_1 - 1)}{\epsilon_1 + 2} + \frac{(1 - f_1^v)(\epsilon_2 - 1)}{\epsilon_2 + 2}, \quad (5)$$

where ϵ_e is the "effective" dielectric constant of the mixture, f_1^v is the volume fraction of medium 1 ($f_1^v + f_2^v = 1$), and ϵ_1 and ϵ_2 are ϵ for medium 1 and 2, respectively. The expression for Bruggeman is

$$\frac{f_1^v(\epsilon_1 - \epsilon_e)}{\epsilon_1 + 2\epsilon_e} + \frac{(1 - f_1^v)(\epsilon_2 - \epsilon_e)}{\epsilon_2 + 2\epsilon_e} = 0. \quad (6)$$

The Debye and Bruggeman expressions are symmetric with respect to the two media. Maxwell–Garnett differs in this respect as this rule makes a distinction between the

AMTD
7, 12873–12927, 2014

"matrix" ($\epsilon = \epsilon_m$) and the "inclusion" ($\epsilon = \epsilon_i$):

$$\epsilon_e = \epsilon_m + 3f_i^v \epsilon_m \frac{(\epsilon_i - \epsilon_m)}{\epsilon_i + 2\epsilon_m - f_i^v(\epsilon_i - \epsilon_m)}, \quad (7)$$

where is f_i^v is the volume fraction of the inclusion medium ($f_m^v + f_i^v = 1$). That is, for Maxwell–Garnett we have two cases "air in ice" and "ice in air", below shortened to MG_{ai} and MG_{ia}, respectively, that result in different ϵ_e depending on if air is set to be the matrix or inclusion medium.

For completeness, the effective density (ρ_e) matching f_1^v is

$$\rho_e = f_1^v \rho_1 + (1 - f_1^v)\rho_2, \quad (8)$$

where ρ_1 and ρ_2 are the density of medium 1 and 2, respectively. In terms of mass fraction of medium 1 (f_1^m), ρ_e is

$$\rho_e = \frac{\rho_1 \rho_2}{f_1^m \rho_2 + (1 - f_1^m)\rho_1}. \quad (9)$$

An example comparison between the mixing rules is shown in Fig. 2. A first observation is that the Debye and the "ice in air" version of Maxwell–Garnett (MG_{ia}) give identical results (for $\epsilon_m = \epsilon_{air} = 1 + i0$ the two formulas are mathematically identical). Hence, the Debye rule is not explicitly discussed below, but is represented by the identical MG_{ia}. MG_{ia} gives consistently the lowest refractive index, for both real and imaginary part. The difference to the other two rules is the highest at air fractions around 0.45. The highest values are throughout found for MG_{ai}, and Bruggeman falls between the two Maxwell–Garnett versions. Repeating the calculations for other frequencies and temperatures (e.g. Johnson et al., 2012, Fig. 2), i.e. other ice refractive indices, shows that these patterns are of general validity, and are not specific to our example.

The deviations between the mixing rules are significant. For example, Johnson et al. (2012) conducted a sensitivity analysis for frequencies between 2.8 and 150 GHz regarding the choice of mixing rule. The differences when using MG_{ai} or MG_{ia} were found to be ~ 2 dB for radar reflectivity and reach at least 10 K for brightness temperature.

AMTD
7, 12873–12927, 2014

Some mixing rule can be optimal for representing a true homogeneous ice-air spherical particle, as studied by Petty and Huang (2010), but this is not the crucial point in this context. In Sect. 5.1 we instead pragmatically test if any of the mixing rules leads to a simpler approximation of realistically shaped particles.

3 Existing DDA databases

The Discrete Dipole Approximation (DDA) is the most widely used method for computing the scattering properties of arbitrarily shaped particles. In the DDA method, a particle is represented by an array of dipoles in a cubic lattice with a given inter-dipole spacing. This spacing must be adequately small relative to the incident wavelength in order to obtain desired accuracy, which requires large computer memory and long calculation time for large particles.

Despite the wide usage of the method, the publicly available DDA data for microwave scattering of ice particles are limited. The three databases that are used in this study are the ones of Liu (2008); Hong et al. (2009) and Nowell et al. (2013). The main properties of these databases are summarised in Table 1.

The only other open source of microwave DDA data that we know about is www.helsinki.fi/~jktyynel/database.html, where data used in Tyynelä and Chandrasekar (2014) and some other publications were recently made available. These data, covering frequencies up to 220 GHz, are not included in this paper as they deal with partly oriented particles, while the other databases all are valid for completely random orientation.

3.1 Liu

Liu (2008) applied the DDA code of Draine and Flatau (2000), denoted as DDSCAT, and computed single scattering properties (i.e. scattering cross section, absorption cross section, back-scattering cross section, asymmetry parameter, and phase function) of

AMTD
7, 12873–12927, 2014

eleven types of ice particle crystal shapes, at 22 frequencies (3, 5, 9, 10, 13.4, 15, 19, 24.1, 35.6, 50, 60, 70, 80, 85.5, 90, 94, 118, 150, 166, 183, 220 and 340 GHz) and for five different temperatures. To not clutter the figures below, we include only six of the eleven particle types. The ignored shapes are: short column, block column, thin plate and 4 and 5-bullet rosettes; included shapes are pointed out in the figure legends.

The particles were treated to have random orientation. The phase function is provided for 37 equally spaced scattering angles between 0 and 180°. In terms of the "phase matrix" required for vector radiative transfer, only the (1,1) element is given. The refractive index of ice applied in the DDA calculation was taken from Mätzler et al. (2006).

3.2 Nowell

A new snowflake aggregation model is introduced in Nowell et al. (2013). The 6-bullet rosette is a frequently observed crystal shape and therefore was selected by Nowell et al. (2013) as constituent crystals of the simulated snowflake aggregates. The aggregates were allowed to grow in three dimensions, following an algorithm resulting in quasi-spherical snowflakes following the diameter-density parameterisation of Brandes et al. (2007). The representation of the bullet rosettes is somewhat coarse, based on cubic blocks with size of ≈ 50 µm. Only particles with a maximum diameter above 1 mm are included in our figures to make sure that the aggregates consist of a relatively high number of building blocks.

The single scattering properties of an ensemble of randomly generated aggregates were calculated by the DDSCAT code. Calculations for ten frequencies (10.65, 13.6, 18.7, 23.8, 35.6, 36.5, 89, 94, 165.5, and 183.31 GHz) and a single temperature (263 K) were performed, with refractive index taken from Mätzler et al. (2006). The phase function is not included in this database, only the corresponding asymmetry parameter is stored.

AMTD
7, 12873–12927, 2014

3.3 Hong

Also Hong et al. (2009) used DDSCAT, to compute the scattering properties (extinction efficiency, absorption efficiency, single scattering albedo, asymmetry parameter, and scattering phase matrix) of six randomly oriented non-spherical ice particles at 21 frequencies (90, 118, 157, 166, 183.3, 190, 203, 220, 243, 325, 340, 380, 425, 448, 463, 487, 500, 640, 664, 683, and 874 GHz) for a temperature of 243 K. All six independent elements of the phase matrix are reported, in steps of 1° between 0° and 180°.

The geometrical information of the six ice particle shapes is detailed in Table 1 of Hong (2007). To obtain the properties of randomly oriented particles, β, θ, and φ are varied in ranges of $0-2\pi$, $0-\pi$, and $0-2\pi$, and scattering quantities are averaged over different combinations of orientations. Refractive index of ice was taken from Warren (1984), that according to Sect. 2.1 is not the optimal choice with respect to particle absorption.

3.4 Comparison of the databases

Example DDA data are found in Fig. 3, for one of the few frequencies that is found in all three databases (183 GHz). All three aggregate types in the Nowell database are plotted with the same symbol. The abscissa of the figure is size parameter according to Eq. (2), implying that the radiative properties are compared between particles having the same mass. Absorption, scattering and back-scattering are reported as the corresponding efficiency, Q, calculated with respect to d_e as

$$Q = \frac{4\sigma}{\pi d_e^2}, \tag{10}$$

where σ is the cross-section of concern. Even though usage of Q provides some normalisation of the data, compared to if cross-sections would be plotted, the ordinates in the first three panels of Fig. 3 still span several orders of magnitude. In Fig. 4 another normalisation is applied, that brings out differences at lower size parameters:

AMTD
7, 12873–12927, 2014

The optical cross-sections are divided by the corresponding optical cross-section of the equivalent mass solid ice sphere with same ice refractive index.

Although we discuss the soft particle approximation in depth only in Sect. 5, solid and soft spheroids are already included in the figures here for reference. We also already make some remarks on their optical properties here, but postpone the explanation of how the soft-spheroid results were generated to the dedicated section later.

The Hong data have systematically a higher absorption than Liu. This can be discerned in Fig. 3 and is expected due to the higher imaginary part of the refractive index (n'') in W84 (used by Hong) compared to M06 (used by Liu) for frequencies below 400 GHz, as shown in Fig. 1. This deviation is removed in Fig. 4 as the normalisation is done with respect to Mie calculations with the refractive index set to match the DDA data. Without this adjustment of the refractive index, there would be a much higher variability in the absorption ratios in Fig. 4, with the different DDA databases at different mean levels. Droxtal particles are quasi-spherical and the fact that these particles obtain ratios very close to one in Fig. 4 confirms that a correct normalisation has been applied. This similarity in shape explains also why the droxtals end up close to the data for solid spheres for all quantities in Fig. 3.

It is well known that the impact of shape on the extinction efficiency increases with particle size. Accordingly, for x below ~ 0.5 there is a comparably low spread between different particles, for both absorption and scattering. In terms of the ratio in Fig. 4, the data are mainly inside 1.2 ± 0.2. On the other hand, at $x = 2$ the difference between the lowest and highest scattering, for particles having the same mass, is about a factor of five (Fig. 3). These remarks consider also 340 GHz (not shown) where the same particles result in higher size parameters.

The back-scattering efficiency shows a similar pattern as the scattering one, but the variation above $x = 2$ is considerably higher, about a factor of ten. This is the case as the back-scattering depends on the phase function for a particular direction, resulting in a higher sensitivity to the exact shape of that function, while the overall scattering extinction corresponds to the integrated phase function.

AMTD
7, 12873–12927, 2014

There is a significant spread in the asymmetry parameter (g) from about $x = 0.5$ and above. Above $x \approx 1.5$, the difference between highest and lowest g is about 0.3, where the Nowell aggregates and the Liu bullet rosettes throughout cause the highest and lowest values, respectively. The 6-bullet rosettes in the Hong database show the same tendency of low g for combinations of size and frequency resulting in $x > 1.5$. On the other hand, at lower x the Hong rosettes tend to give the highest g among all of the particles, then also higher than the corresponding Liu rosette. That is, the different 6-bullet rosette models used by Liu and Hong result in significantly different optical properties.

Figure 3 was inspired by Fig. 7 of Nowell et al. (2013), comparing that database with solid and soft particle calculations in the same way. Nowell et al. (2013) used a higher air fraction for their soft particles and it is not clear if the MG_{ai} or MG_{ia} version of the Maxwell–Garnett mixing rule was used, but there are still some clear deviations between the two figures for soft particles. For example, the scattering efficiency of soft particles in our Fig. 3 is quite close to the data from Nowell et al. (2013), while in their Fig. 7 the soft particles give significantly lower scattering. In addition, we obtain basically identical scattering efficiencies for soft spheres and spheroids, while Nowell et al. (2013) got lower scattering for spheroids. We have carefully checked our calculations and our results seem to fit better with what has been found elsewhere. For example, in Fig. 5 of Liao et al. (2013) a good agreement with the aggregates of Nowell et al. (2013) is obtained by soft particles having a density of $0.2\,g\,m^{-3}$ (the air fraction of 0.75 in Fig. 3 matches $0.23\,g\,m^{-3}$), and basically identical results are obtained between spheres and both prolate and oblate spheroids.

4 Relevance of absorption and asymmetry parameter

To judge the performance of a soft particle approximation or some "shape model", a basic consideration is in what detail the single scattering properties must be compared? The main issue is that the phase function (describing the angular redistribution of scat-

AMTD
7, 12873–12927, 2014

tered radiation, also denoted as the scattering function) can be very complex and is basically unique for all particles where not Rayleigh conditions apply. However, it is normally not required to compare the phase function in full detail. For example, it is in general only the direct back-scattering that is of interest for radar applications. This is valid until multiple scattering becomes significant, when also the phase function starts to be relevant.

For passive measurements, the standard choice is to give an overall description of the phase function by using the parameter g. The asymmetry parameter is known to have a strong influence in radiative transfer of solar radiation (e.g. Kahnert et al., 2008). The quantity is also frequently reported in connection to passive microwave radiative transfer (e.g. Liu, 2004; Kim, 2006), but, to our best knowledge, the actual influence of g for such applications has not been investigated in a general manner. A simple test of this type is found in Fig. 5. Satellite measurements at 150 GHz and an incidence angle of 45° were simulated. Temperature and gas profiles were taken from a standard tropical scenario (Fascod), and a 2 km thick "cloud" layer, centred at 10 km, was added. A single particle size (monodispersive PSD) was used for each simulation, and the number of particles was adjusted to obtain the specified zenith optical depths. Spherical particles with an air fraction of 0.4 were assumed, and d_e was varied to obtain a range of g.

The solid lines in Fig. 5 show how the radiance changes with g when the cloud optical depth is kept constant and all particle absorption is suppressed. The basic pattern is that the cloud impact on measured radiance decreases with increasing g. This makes sense as high g means that the up-welling emission from the lower troposphere is less redirected, compared to the case of more isotropic scattering at low g. See Buehler et al. (2007) for a schematic figure and discussion of the radiative transfer for this measurement geometry. It is hard to see in the figure, but there actually are some "wiggles" around $g = 0.65$, showing that the relationship to g is not completely monotonic. That is, several values of g can result in the same radiance.

AMTD
7, 12873–12927, 2014

In Fig. 5 the cloud impact for $g = 0$ and $g = 0.6$ differs by a factor of about 2. That is, changing g with 0.1 results in a $\sim 10\,\%$ change in cloud impact. For low optical thickness the relationship between scattering cross-section (σ_s) and radiance impact is close to linear. Accordingly, a 10 % error in σ_s and a 0.1 error in g are in rough terms equally important. The test displayed in Fig. 5 was repeated for other frequencies and cloud altitudes. The absolute values of the cloud impact change, primarily following the magnitude of the gas absorption at the altitudes around the cloud layer, but the mentioned relation between σ_s and g was found to be relatively constant.

There is also some uncertainty regarding the importance of ice particle absorption for passive measurements. It is well known that absorption is most significant for smaller particles, i.e. the single scattering albedo increases with particle size (e.g. Evans and Stephens, 1995b; Eriksson et al., 2011b). Figure 5 confirms this as the difference between considering absorption (dashed lines) and neglecting it (solid lines) is high for small x, for all cloud optical depths. This aspect is especially important for limb sounding, as in this observation geometry focus is put on higher altitudes where smaller particles are more frequent, and it has been shown that the measured signal can even be dominated by absorption (Wu et al., 2014).

Figure 5 shows also the less obvious fact that absorption increases in importance with increasing cloud optical thickness. For an optical thickness of 2.0 absorption is significant up to at least $x = 1.2$, while for small optical depths (such as 0.1) the absorption can be neglected for x above ~ 0.5. This is a consequence of that the probability of absorption increases when multiple scattering becomes more prominent. The changed conditions caused by multiple scattering implies that the relevance of absorption can not be judged alone from the single scattering albedo parameter. In addition, the observation geometry matters for the relative importance of absorption and scattering, as discussed in Eriksson et al. (2011b).

In summary, it is confirmed that the quantities normally considered (σ_a, σ_s, σ_b, and g) are all relevant, but to a varying degree. Most importantly, the relevance of absorption decreases with size parameter.

AMTD
7, 12873–12927, 2014

5 Approximation by soft particles

The soft particle approach (SPA) is based on two main simplifications. Firstly, the particle is treated to consist of a homogeneous mix of air and ice, and also water if mixed-phase particles are considered (e.g. Galligani et al., 2013). The air fraction of the mix is either set to a constant value, or is obtained by assuming an effective density of the particle, likely varying with particle maximum size. A single refractive index is assigned to the mix by applying a mixing rule (Sect. 2.2). Secondly, the particles must be set to have some specific shape, to allow that the single scattering properties can be determined with a limited calculation burden. As mentioned, the T-matrix method allows that e.g. soft columns and plates are possible options, but the standard choices are to model the particles as spheres or spheroids. A much more careful description of SPA is provided by Liao et al. (2013).

5.1 Selection of mixing rule

As a first step, we examined if the choice of mixing rule is critical in any way for SPA. The difference between mixing rules can in general be compensated by selecting different air fractions, but exceptions exist. This is most clearly seen for the absorption and scattering cross-section at smaller x, as exemplified in Fig. 4. In the figure, the absorption of soft particles when using Maxwell Garnet with "ice in air" (MG_{ia}) is throughout lower than the DDA results. This in contrast to when using the Bruggeman or the "air in ice" version of Maxwell Garnett mixing rule (MG_{ai}), where the soft particle absorption matches some of the DDA data points. The same pattern is found also for the scattering cross-section, but for a smaller range of x.

The low bias in Fig. 4 of MG_{ia}, compared to DDA data, can not be removed by modifying the air fraction, as shown in Fig. 6. In this figure, the ratios of Fig. 4 are calculated for air fractions between 0 and 0.95 and the ratios obtained when using MG_{ia} are throughout below 1. Ratios around at least 1.2 are required to represent the average values of the DDA data in Fig. 4. For $x < 0.5$ such ratios, and even much

AMTD
7, 12873–12927, 2014

higher values, can be obtained by selecting the MG_{ai} mixing rule. Ratios when using Bruggeman (not shown) reach 1.25 for absorption and 1.15 for scattering, which is on the limit to fit the DDA data. For MG_{ai} the ratios switch from being > 1 to < 1 around $x = 1$, that below is shown to be the general behaviour of DDA data.

The conclusion of Figs. 4 and 6 is that using the MG_{ia} mixing rule leads to a systematic underestimation of the absorption and scattering at some size parameter ranges. The same applies to the Debye mixing rule as it is identical to MG_{ia}. The Bruggeman rule gives higher values, but is not capable of reproducing the highest DDA-based ratios found in Fig. 4. These remarks do not depend on if soft spheres or spheroids are used. Accordingly, MG_{ai} appears as the best choice in this context, and only this mixing rule is considered below.

5.2 Selection of particle shape

Solid spheres are known to exhibit resonance features for x above ~ 1, which are reflected as oscillations in the properties displayed in Fig. 3 (blue solid lines). An individual spheroid would give similar oscillations, but the assumption of completely random orientation partly averages out those patterns for the spheroids (see Fig. 3, red solid lines). The resonance phenomena are dampened when going to soft particles. This results in a marginal difference in extinction (absorption and scattering cross-sections) and g between soft spheres and spheroids (dashed lines). However, there is a significant difference for the back-scattering, where soft spheres give even stronger oscillations than solid spheres. The soft spheroids show a more smooth variation with x, and should allow a better fit to the DDA data. Liao et al. (2013) made the same observations for soft particles, and showed that extinction and g are basically unaffected by the aspect ratio of the spheroids, or if they are oblate or prolate. They found also that the oscillations in size dependence of the back-scattering decrease when the aspect ratio moves away from one.

That is, soft spheroids are to prefer over soft spheres, primarily due to the difference with respect to back-scattering. For complete random orientation the selection

AMTD
7, 12873–12927, 2014

of aspect ratio is not critical, and only oblate spheroids with an axial ratio of 0.6 are considered below, following Hogan et al. (2012). In terms of the nomenclature used in the T-matrix code, this equals an aspect ratio of 1.67.

5.3 Selection of air fraction

As shown in the above figures, for a given size parameter there is a spread of the particle optical properties over the different habits. Hence, it is not possible to match all particle shapes on the same time with a soft particle approximation. The ambition is instead to approximately mimic the average properties. Figure 3 shows that solid spheres and spheroids do not meet this criterion as they e.g. for $x > 4$ systematically underestimate scattering cross-section and g.

5.3.1 Relevance of the reference data

A more detailed analysis requires some consideration of the occurrence frequency of the different particles in the DDA databases. For example, the Hong database contains droxtals having a maximum diameter, d_m, up to 2 mm, while the general view is that this shape is only representative for smallest ice crystals (Baran, 2012). In fact, Schmitt and Heymsfield (2014) found that cloud ice particles with a d_m above 250 µm are mainly of aggregate type, implying that also single plates and columns having dimensions above this size are relatively rare. The aggregate types discussed by Schmitt and Heymsfield (2014) appear to be relatively similar to the aggregates in the Hong database.

For the representation of particles of snow type, the Liu database offers two shapes (dendrite and sector-like snowflakes) both having high aspect ratios, while the aggregates of the Nowell database (claimed to represent snowflakes) have an aspect ratio close to 1. This difference in aspect ratio results particularly in deviations in the scattering cross-section and g of those particles (Fig. 3). If "snow" is understood as everything from the classical single-crystal snowflake to graupel, both these assumptions on aspect ratio are realistic, but it is clear that particles having intermediate aspect ratios

AMTD
7, 12873–12927, 2014

also exist and, hence, they are not yet covered by the DDA databases. The Hong aggregates could potentially also work as proxy for snow particles, but data for d_m above 2 mm are lacking.

5.3.2 Fit of single scattering data

Figure 3 exemplifies a fit of the available DDA data using soft particles having an air fraction (AF) of 0.75. For the frequency of concern (183 GHz) the soft particles, compared to the solid ones, give indeed a better general fit of absorption and scattering efficiencies. For g at $x > 1.5$, the soft particles agree well with the Nowell aggregates, while all other particle shapes are better approximated with solid spheres or a comparably low AF. That is, for e.g. the Liu sector-like snowflake, the AF that gives the best fit with scattering efficiency is not the same AF that is needed to match g.

Example results for other frequencies are found in Fig. 7. This figure, together with Fig. 4 covering 183 GHz, indicate that the MG_{ai} mixing rule combined with an AF of 0.25 give an acceptable fit of absorption and scattering for size parameters below 0.5, independently of frequency. At higher x, AF = 0.25 is not optimal, it gives a fairly good fit at 874 GHz (Fig. 7), but at e.g. 90 GHz this AF results in too high values for both absorption and scattering. For $x > 1$ and lower frequencies, a fit of absorption and scattering efficiencies requires higher AFs. For example, mimicking the scattering efficiency at 90 GHz requires an AF on the order of 0.75–0.9, depending on if all or just snow-type particles should be fitted.

These remarks show three facts. Firstly, there is in general not a single AF that simultaneously gives a fit of all four optical property parameters. Secondly, at least when operating at lower frequencies, the AF to apply in a soft particle approximation must be allowed to vary with particle size. Thirdly, the best AF has a frequency dependence (at least for larger x). The third point is well-known, it has been shown by e.g. Liu (2004).

The soft particle AF is frequently set to follow some density parameterisation. This gives the AF a variation with size in line with the second point. However, already the known fact that an optimal AF varies with frequency (point 3) signifies that using true

AMTD
7, 12873–12927, 2014

densities can not work as a general approach with respect to optical properties. This is the case as density-based AFs are independent of frequency. In addition, for larger particles standard density parameterisations result in much higher AFs than the ones giving a match of single scattering data around 100 GHz and above. As an example, the particle model of Hogan et al. (2012) is included in Fig. 7. This particle model is based on the frequently used density parameterisation of Brown and Francis (1995), that leads to AFs close to 1 for the largest DDA particles. In fact, the scattering efficiency at 90 GHz becomes too low already at $x \approx 0.5$. Also, back-scattering is underestimated at x above ≈ 0.5, even at lower frequencies (Fig. 8). All other density parameterisations we have tested show the same general feature, to produce, in this context, too high AFs for larger particles. For more recent parameterisations the density goes below $100\,\mathrm{kg\,m^{-3}}$ at $d_\mathrm{m} \approx 800\,\mu\mathrm{m}$ (Cotton et al., 2013, Fig. 6).

Hogan et al. (2012) was selected as it provides a clearly defined particle model. However, it should be noted that Hogan et al. (2012) treat the spheroids to be aligned with the maximum dimension in the horizontal plane, while we apply completely random orientation.

5.3.3 Test radiative transfer simulations

Absorption, scattering and asymmetry parameter interact for simulations of passive observations, as shown in Sect. 4. Some test simulations were performed in order to check if the different tendencies for these quantities combine in a positive or negative manner. These simulations, shown in Fig. 9, were performed for the same scenario as used for Fig. 5. Again, a monodispersive PSD was used, but here the number of particles was adjusted to obtain a specified vertical column of ice mass, or ice water path (IWP). The IWP for each frequency was selected to give a maximum cloud induced brightness temperature change of 5–10 K, in order to get a significant response but still avoiding a high degree of multiple scattering.

The calculations were done with the DOIT module of the ARTS radiative transfer model (Emde et al., 2004; Eriksson et al., 2011a), that requires the full phase function

AMTD
7, 12873–12927, 2014

and no results for the Nowell database could be generated. For Fig. 9 a more strict selection of the DDA particles was done, roughly matching the discussion in Sect. 5.3.1 in order to just keep the most realistic particles. Column, plates and 3-bullet rosettes having d_m above 1 mm were excluded. For droxtals the limit was set to 200 µm. The black solid lines show a polynomial fit (in linear scale) of the simulations based on the remaining DDA particles.

As expected from the discussion above, the different DDA particles give little spread of simulated brightness temperatures for $x < 0.5$. On the other hand, there is a strong variation at larger size parameters. For example, the Liu dendrite snowflakes, and around $x = 1$ also the Hong 6-bullet rosettes, have particularly low influences. This is a combined effect of relatively low scattering efficiency and high g (Fig. 4). The same combination enhances also the differences between the Liu sector-like and dendrite snowflakes, compared to the differences for scattering efficiency alone. The relative influence between the particles is not the same for all frequencies. For example, the Hong aggregates are found on the high side for 90 and 166 GHz, but are rather on the low side for 874 GHz.

Figure 9 shows that the selection of the soft particle AF is not highly critical for size parameters below 0.5. This is partly due to compensating errors. A too high AF gives an overestimation of both absorption and scattering, but this is counteracted by an overestimation of g. At higher size parameters, the frequency dependence of the "optimal" AF noted above is seen also here. For example, at 340 GHz, an AF of 0.25–0.50 is required to match the fit of the DDA results (black line), while for 90 GHz a suitable AF is above 0.75. For 874 GHz, only covered by the Hong database, an AF around 0.25 gives best agreement. The systematic deviation between the soft particle and the DDA-based results seen for 874 GHz and low x is due to the refractive index differences discussed in Sect. 2.1.

AMTD
7, 12873–12927, 2014

6 Approximation by a single representative shape

Based on poor experience of using the SPA at ECMWF (the European Centre for Medium-Range Weather Forecasts), Geer and Baordo (2014) attacked the representation of particle shape in microwave radiative transfer from another angle. Their application is data assimilation for numerical weather prediction, but the basic problem is the same as for direct retrieval of frozen hydrometeors. Their approach is simple, to try to find a particle type, for which DDA calculations are at hand, that minimises the average deviation to actual observations. They compared to measurements from the TMI and SSMIS sensors, for frequencies between 10 and 190 GHz. The Hong database does not cover the lower end of this frequency range, and only the Liu database was considered.

They performed global simulations, for latitudes between 60° S and 60° N. Simulated brightness temperatures were obtained with RTTOV-SCATT, a radiative transfer tool making use of several approximations. The atmospheric data were taken from the ECMWF 4D-var assimilation system, likely having biases in ice mass amounts varying between regions, land/ocean and the different hydrometeor types. Further, a PSD must be assumed for the simulations. The tropical version of the PSD of Field et al. (2007) was found to give the best overall fit with observations, among the three PSDs considered. These aspects introduce problems for a clear identification of the best overall proxy particle shape, as discussed in detail by Geer and Baordo (2014).

The final recommendation of Geer and Baordo (2014) is to apply the Liu sector-like snowflake, for all classes of both cloud ice and snow. A somewhat better fit could be obtained by some combinations involving the 6-bullet rosettes and dendrite snowflake particles, but the improvement was not sufficiently large to motivate a more complicated particle shape model. Our results corroborate the selection of the sector-like snowflake as the general proxy shape particle. First of all, this particle type does not stand out in any obvious way, it shows in general intermediate values. In fact, the best match with the polynomial fit of the DDA-based simulations in Fig. 9 (black lines) is given by the

AMTD
7, 12873–12927, 2014

sector-like snowflakes for both 90 and 166 GHz. A good fit is also obtained by the Liu 6-bullet rosette, another particle type that Geer and Baordo (2014) had as a strong candidate. The sector-like snowflake tends to be on the high end for x around 0.7, but on the low side at higher x. If these happen to be true biases, they are partly averaged out in PSD-weighted bulk properties.

The Liu sector-like snowflakes exhibit average properties also at 340 GHz, above the frequency range considered by Geer and Baordo (2014). The pattern is very similar to the lower two frequencies, with some tendency to "overshooting" around $x = 1$. If the upper limit for plates and columns would have been set to a lower value, such as 500 µm, the sector-like snowflakes would even have shown outlier behaviour around $x = 1$. This results in that for 340 GHz an even better agreement with the polynomial fit is obtained with the Hong aggregates. This particle type is throughout below the fitting line at 874 GHz, but this result depends heavily on a strong influence on the polynomial fit of columns and plates with $d_e \approx 500$ µm. The Hong bullet rosette seems not to be a candidate for the role as general proxy shape because it has a very low scattering efficiency around $x \approx 1.5$, which is also reflected in Fig. 9.

Figures 2 and 3 of Geer and Baordo (2014) complement the figures of this paper by reporting bulk optical properties of the Liu particles as function of ice mass and frequency. A bit surprising is that the sector-like snowflake is found to have the lowest bulk g, seemingly for all frequencies and ice masses. This shape has also the lowest g among the Liu particles in Fig. 3, but only up to $x = 1$. On the other hand, the SPA spheres applied are found to give very high bulk g. Geer and Baordo (2014) explain this as a result of the Mie theory, but according to our Fig. 3 the high g is rather a result of the low density assumed. The snow hydrometeor class is set to have a density of 100 kg m^{-3}, corresponding to an AF ≈ 0.9. We can not easily judge the exact impact of this high AF for several reasons, e.g. Geer and Baordo (2014) used a mixing rule not considered by us. Another complication is that the Field et al. (2007) PSD operates with d_m. Hence, also differences in the relationship between particle mass and d_m between

AMTD
7, 12873–12927, 2014

the particles affect the data derived by Geer and Baordo (2014). There is a much more intuitive mapping of our findings to bulk properties if the PSD is based on d_e.

Geer and Baordo (2014) analysed only passive observations, while it would be highly beneficial if the representative shape selected also can be applied for radar measurements. Figure 8 indicates that this is the case. The back-scattering of the sector-like snowflake follows its pattern for the scattering efficiency (Fig. 7). This shape has a ratio (as defined in discussed figures) above one up to a somewhat higher size parameter than the other particles, more pronounced at 35.6 GHz than at 94 GHz, but besides this, its properties are of average character also with respect to back-scattering.

7 Is using maximum dimension a better option?

Up to this point, we have compared radiative properties between particles having equal d_e (thus also having the same mass), for reasons discussed in the introduction. The second main measure for the size of individual particles is the maximum dimension, d_m. In fact, there are likely more particle size distributions (PSDs) using d_m than d_e. Hence, it is useful to also understand how the radiative properties vary with d_m, and such an overview for 183 GHz is given in Fig. 10. This figure was produced as Fig. 3, but with d_e replaced by d_m in the definition of size parameter and absorption and scattering efficiencies. The panels for asymmetry parameter in Figs. 3 and 10 are quite similar, besides that the range of x is extended when using d_m. On the other hand, there are clear differences for both absorption and scattering efficiencies. There is a much more compact relationship between d_e and these radiative properties than what is found for d_m. In the case of using d_m as size measure, relatively compact particles (droxtals, plates, columns and spheres) obtain especially high absorption and scattering efficiencies, while particles having high aspect ratios (dendrite and sector-like snowflakes) exhibit especially low efficiencies. The stronger influence of particle morphology and aspect ratio causes that the ratio between highest and lowest efficiency is about ~ 100

AMTD
7, 12873–12927, 2014

(besides for smallest particles). This is in clear contrast to Fig. 3, where the same ratios are around or below 10 when using d_e (Sect. 3.4).

However, the higher variability in absorption and scattering efficiencies is not directly mapped to the same variability in bulk optical properties, i.e., the optical properties of the distribution as a whole. The reason for this is that particles with high aspect ratio have a lower mass as a function of d_m. This aspect deserves careful examination, so we analyse it in the remainder of this section. As a measure for the bulk optical properties we select the scattering extinction coefficient.

As an example of a d_m-based PSD we selected the tropical version of the PSD by Field et al. (2007), below denoted as F07. The extinction coefficients were derived with a setup basically identical to the one described by Geer and Baordo (2014), which also used the F07 PSD: only particles with $d_m \geq 100\,\mu m$ were included (as the PSD does not cover smaller particles), and the PSD was rescaled as described in their Appendix C to compensate for the truncation in particle size.

An additional aspect of the Field et al. (2007) size distribution is that it uses two additional input parameters, a and b. They originate from the common way to express the relationship between d_m and particle mass, m, as

$$m = a d_m^b. \tag{11}$$

There are some issues around how to derive a and b for a set of particles, which are discussed in Appendix B of Geer and Baordo (2014). We selected to set the parameters by performing a fit restricted to the particles with $d_m \geq 100\,\mu m$. A reason to ignore the smaller particles in the fit is that for them Eq. (11) may result in $d_m < d_e$ (corresponding to density higher than the one of solid ice) in cases where $b < 3$.

Few d_m-based PSDs take a and b into account. To investigate the impact of this negligence, bulk scattering was also derived with F07 and applying fixed a and b values for all particles, namely $a = 0.069$ and $b = 2$. These are values supported by Wilson and Ballard (1999) and Field et al. (2007). For both fitted and fixed a and b parameters, they

AMTD
7, 12873–12927, 2014

were only used when deriving the F07 PSD, the following calculation steps (including rescaling of the PSD) used the actual particle masses from the DDA database.

Since we want to compare d_m-based and d_e-based bulk extinction coefficients, we also need an example of a d_e-based PSD. For this we selected the PSD by McFarquhar and Heymsfield (1997, below MH97). A comparison between F07 and MH97 is found in Fig. 11, where F07 is rescaled to d_e-basis. Two combinations of a and b are considered where the first combination (0.0015/1.55) matches the sector-like snowflakes, having the lowest b among all the particles in the Liu database, and the second combination (480/3) represents solid spheres and thus also the upper limit of b. The rescaling to match specified ice water content has a marginal impact on F07. On the other hand, MH97 puts a much larger fraction of the mass below 100 µm and the rescaling gives a small but not negligible change, therefore this PSD is displayed both before and after the rescaling. Like F07, MH97 is also a PSD targeting tropical conditions, and the agreement with F07 is relatively high for $a = 0.0015, b = 1.55$, while for $a = 480, b = 3$ the two PSDs deviate strongly.

Using the discussed PSDs, bulk scattering extinction coefficients can be calculated by adding up extinction coefficients for individual particles with appropriate weights. Figure 12 shows the results, total extinction coefficients for the two different PSDs, the d_m-based F07 at the top and the d_e-based MH97 at the bottom. For F07, results for fitted and fixed a and b parameters are shown separately by straight and solid lines, respectively.

As the top panel with the F07 results clearly demonstrates, the general pattern seen for the individual particles (Fig. 10) persists in bulk extinction: The more compact particles are at the upper end and the less compact (more "snowflake-like") particles are at the lower end. However, as expected, the ratio between highest and lowest value is decreased, from ∼ 100 when considering individual particles to ∼ 10 when considering bulk extinction. A similar spread in bulk extinction was obtained by Geer and Baordo (2014, see their Figs. 2 and 3).

AMTD
7, 12873–12927, 2014

Still discussing the top panel of Fig. 12, we now turn to the issue of using fitted or fixed a and b parameters for the F07 PSD. For fixed parameters, the extinction obtained for particular shapes is changed, but the spread of the values is roughly maintained. It should here be noted that keeping a and b fixed only has the consequence that the PSD gets the same basic shape for all particles. The rescaling to ensure that specified mass is matched maintains the relative fraction between particles having different d_m.

While all the discussion so far related to the top panel of Fig. 12, we will now turn to the bottom panel. It shows that particle shape indeed has a much lower impact on bulk scattering for the d_e-based MH97 PSD, compared to the d_m-based F07 PSD. The factor between highest and lowest extinction in case of MH97 is ~ 2.5. This can not be a consequence of that MH97 puts highest weight on completely different particle sizes, as the extinction using MH97 ends up inside the range resulting from F07. Furthermore, the relative variability over the different habits is close to constant with ice water content, for both F07 and MH97, and already Fig. 11 showed that MH97 ends up inside the range covered by F07 when a and b are varied. All in all, F07 and MH97 do a quite similar relative weighting between different particle size ranges. We therefore conclude that the difference in spread seen between upper and lower panel of Fig. 12 is a direct consequence of the fact that the scattering cross-section is more closely linked to d_e than to d_m.

The difference between d_e and d_m, exemplified by Fig. 12, seems to be of general validity for frequencies up to ~ 200 GHz. If anything, the difference increases when going down in frequency (not shown). At higher frequencies a somewhat different pattern is found for the d_m case, as shown in Fig. 13. Here at 340 GHz, the spread in extinction of the different DDA particles is overall lower, compared to Fig. 12, and is particularly low at high ice water content, where it is even smaller than when using d_e. This with the exception of the dendrite snowflake particles, which is maybe an indication that this particular shape should be avoided for higher frequencies. Anyhow, the deviating results for the dendrite snowflake show that the low spread in extinction between the other particles may be a coincidence, not necessarily indicating that using d_m ensures

AMTD
7, 12873–12927, 2014

low uncertainty in extinction for high frequencies and high ice water content. Comparing usage of d_e and d_m at high frequencies is presently complicated by the fact that the Hong database is limited to $d_m \leq 2$ mm, and this size truncation can easily cause artefacts in the comparison.

At the end of this section, we want to briefly mention two more general aspects of the problem to represent bulk particle optical properties. Firstly, our analysis assumed that F07 and MH97 give an equally good representation of the mix of particle sizes. If in situ probes provide better data for either d_e or d_m this should result in higher systematic errors for PSDs based on the more poorly measured particle size.

Secondly, besides possible systematic errors in the PSDs, the variability around average conditions must be considered. For example, it could be the case that there is a lower PSD variation (between locations, day-to-day, etc.) as a function of d_m than as a function of d_e. This situation would decrease, or reverse, the advantage of using d_e. If the opposite was true, that PSDs tend to be more stable in d_e, this would enhance the advantage of selecting d_e in favour of d_m. As far as we know, this important aspect of PSD variability has not been studied so far.

8 Summary and conclusions

We have reviewed the two most established databases of DDA calculations for microwave atmospheric radiative transfer, Liu (2008) and Hong et al. (2009). Nowell et al. (2013) is associated with the Liu database and was also considered. All three databases assume completely random particle orientation. The databases have different frequency coverage, Novel from 10 to 183 GHz, Liu from 3 to 340 GHz, and Hong from 90 to 874 GHz. Liu is the only database providing data for more than one temperature. Scripts to convert the Hong and Liu data to the format expected by the ARTS forward model can be obtained by contacting the authors.

We noted clear systematic differences in absorption between the Hong and Liu databases. The deviations are explained by the fact that the refractive indices are based

AMTD
7, 12873–12927, 2014

on different sources. Hong et al. (2009) used the data from Warren (1984), that now are considered to be outdated. That is, we judge the only easily accessible DDA data above 340 GHz to be inaccurate on particle absorption. In the update of Warren and Brandt (2008), the parameterisation of Mätzler et al. (2006) is recommended for the microwave region, and this is also the source of refractive index used by Liu (2008) and Nowell et al. (2013). Another problematic aspect of the Hong database is the restriction to $d_m \leq 2$ mm.

We mainly compared optical properties between particles having the same mass, and defined the size parameter (x) accordingly (Eq. 2). For small x, below ≈ 0.3, the variation of absorption and scattering between the particles is about 20 % (1.2 ± 0.2 in terms of the ratio used in Figs. 4, 7 and 8). Going towards higher x the variation increases, most quickly for back-scattering, followed by scattering and most slowly for absorption. At higher x, the ratio between lowest and highest value is ~ 10, ~ 5 and ~ 2.5 for those three radiative properties, respectively. The range in scattering is in general generated by the fact that particles of solid types have comparably high scattering, while shapes of "snow" character result in low scattering. Kim (2006) found that solid spheres are representative up to $x = 2.5$ (back-scattering not considered, and clearly allowing some systematic errors), but we, using a larger set of DDA calculations, find that this limit is found somewhere around $x = 0.5$.

We also scrutinised the soft particle approximation (SPA). A first conclusion was that the selection of mixing rule can lead to systematic errors at low x. A mixing rule giving comparably high refractive index, for given air fraction, is needed to avoid this systematic error. We selected the Maxwell–Garnett with ice as matrix and air as inclusion media. With this selection of mixing rule, combined with an air fraction of about 0.25, SPA is applicable up to about $x \approx 0.5$ across the considered frequency range. This gives for absorption and scattering cross-sections a maximum deviation to individual DDA calculations of ≈ 30 %.

On the other hand, usage of SPA at higher x seems problematic. Each individual property calculated by DDA can likely be reproduced by adjusting the air fraction, but

AMTD
7, 12873–12927, 2014

it is in general not possible to achieve a fit with several radiative properties simultaneously. Anyhow, even fitting a single property, such as back-scattering, requires that the air fraction is decreased when moving to higher frequencies. Thus, selecting the air fraction based on some standard density parameterisation can in best case only work in a small frequency range. Our results indicate that this frequency range then is found below 35 GHz as this approach leads to high AFs, passing 0.9 at $d_m \sim 1$ mm. At very high frequencies, such as 874 GHz, an air fraction of 0.25 could potentially be applied for all particle sizes, but at lower frequencies the air fraction must also be adjusted with size, from about 0.25 at low x (see paragraph above) to a higher value at higher x, for example, 0.7–0.9 at 90 GHz. That is, applying SPA across the microwave region requires a model with a high number of tuning variables, to give the air fraction the needed variation with frequency and size, while at the same time the resulting particle densities have no physical basis.

Inspired by Geer and Baordo (2014), we investigated also a second way to represent average radiative properties. The idea is simple, if any of the particles covered by the DDA databases exhibits average properties, use this particle shape to represent true habit mixes. Geer and Baordo (2014) compared the particles of the Liu database using real passive observations, but they were then forced to involve assumptions on particle size distribution (PSD) and ice mass concentration, while we mainly compared the basic radiative properties directly. However, some radiative transfer calculations were required to assess how differences in scattering cross-section and asymmetry parameter combine in simulations of downward-looking passive measurements, but these calculations did not involve any additional assumptions. The critical part in our approach is the judgement how representative the different DDA particles are with respect to the mean conditions in the atmosphere.

Due to the lack of reference data, we selected to not push the analysis too far at this point and discussed only in general terms which particle shapes show overall average properties. It is of course possible to use the same methodology to, e.g., select a rep-

AMTD
7, 12873–12927, 2014

resentative shape separately for “cloud ice” and “snow”, or targeting different cloud types.

Interestingly, both Geer and Baordo (2014) and we find that the sector-like snowflake particles, among the shapes found in the Liu database, best represent average properties. This was found valid also for higher frequencies than considered by Geer and Baordo (2014), as well as for application in radar retrievals. For frequencies above 340 GHz, where the selection is restricted to the Hong database, an aggregate model appears to be a suitable choice. However, solid conclusions can not yet be drawn, as the amount of reference data so far is quite limited. More data of optical properties of aggregate and snow-type particles are needed to get a more robust basis for studies like this. In its turn, this requires new algorithms for generating realistic particle models, to be used as input to DDA or similar calculation methods. If new databases are created, the limitations of present databases in temperature, particle size, and frequencies should be avoided.

Besides the “shape model”, we also investigated the representation of particle size. Most importantly, it is demonstrated that there is a much more compact relationship between absorption and scattering properties with mass equivalent diameter (d_e) than with maximum dimension (d_m). With the exception of small x, the spread of absorption and scattering efficiencies is at least a factor of 10 higher when d_m is used to define the size parameter, compared to when using d_e. The difference is decreased when summing up individual values to obtain bulk properties, but using a d_m-based PSD gives still a higher uncertainty in the extinction for a given ice water content compared to using a d_e-based PSD. Below 200 GHz, the uncertainties are roughly a factor 10 and 3 for the d_m and d_e case, respectively. Scattering extinction at 340 GHz shows a somewhat different pattern, and perhaps indicates that the difference between d_m and d_e could vanish at even higher frequencies. In any case, it would be highly beneficial if future in-situ measurement campaigns could target to provide PSDs in terms of d_e, such measurements seem to be much less frequent than ones of d_m.

AMTD
7, 12873–12927, 2014

Finally, we stress that the entire study was performed assuming completely random particle orientation. This is probably the main limitation of the conclusions made above. It can not be ruled out that, e.g., the spread of scattering and the difference between using d_m and d_e is highly dependent on particle orientation. That is, a main consideration for future databases of ice hydrometeor optical properties is to make it possible to study the radiative properties when assuming different distributions of horizontal orientation.

Acknowledgements. Financial support for this study was provided by the Swedish National Space Board. Furthermore, we want to express our high appreciation to the persons behind the publicly available DDA databases. Michael Kahnert, Bengt Rydberg and Manfred Brath are thanked for helpful comments.

References

Austin, R. T., Heymsfield, A. J., and Stephens, G. L.: Retrieval of ice cloud microphysical parameters using the CloudSat millimeter-wave radar and temperature, J. Geophys. Res., 114, D00A23, doi:10.1029/2008JD010049, 2009. 12876

Baran, A. J.: From the single-scattering properties of ice crystals to climate prediction: a way forward, Atmos. Res., 112, 45–69, 2012. 12893

Baran, A. J., Connolly, P. J., Heymsfield, A., and Bansemer, A.: Using in situ estimates of ice water content, volume extinction coefficient, and the total solar optical depth obtained during the tropical ACTIVE campaign to test an ensemble model of cirrus ice crystals, Q. J. Roy. Meteor. Soc., 137, 199–218, 2011. 12876

Bauer, P., Moreau, E., Chevallier, F., and O'keeffe, U.: Multiple-scattering microwave radiative transfer for data assimilation applications, Q. J. Roy. Meteor. Soc., 132, 1259–1281, 2006. 12877

Bennartz, R. and Petty, G. W.: The sensitivity of microwave remote sensing observations of precipitation to ice particle size distributions, J. Appl. Meteorol., 40, 345–364, 2001. 12877

Boukabara, S.-A., Garrett, K., Grassotti, C., Iturbide-Sanchez, F., Chen, W., Jiang, Z., Clough, S., Zhan, X., Liang, P., Liu, Q. Islam, T., Zubko, V., and Mims, A.: A physical approach for a simultaneous retrieval of sounding, surface, hydrometeor, and cryospheric parameters from SNPP/ATMS, J. Geophys. Res., 118, 12–600, 2013. 12876

AMTD
7, 12873–12927, 2014

Brandes, E. A., Ikeda, K., Zhang, G., Schönhuber, M., and Rasmussen, R. M.: A statistical and physical description of hydrometeor distributions in Colorado snowstorms using a video disdrometer, J. Appl. Meteorol. Clim., 46, 634–650, 2007. 12885

Brown, P. R. and Francis, P. N.: Improved measurements of the ice water content in cirrus using a total-water probe, J. Atmos. Ocean. Tech., 12, 410–414, 1995. 12895

Bruggeman, V. D.: Berechnung verschiedener physikalischer Konstanten von heterogenen Substanzen. I. Dielektrizitätskonstanten und Leitfähigkeiten der Mischkörper aus isotropen Substanzen, Ann. Phys. (NY), 416, 636–664, 1935. 12882

Buehler, S. A., Jiménez, C., Evans, K. F., Eriksson, P., Rydberg, B., Heymsfield, A. J., Stubenrauch, C., Lohmann, U., Emde, C., John, V. O., Sreerekha, T. R., and Davis, C. P.: A concept for a satellite mission to measure cloud ice water path and ice particle size, Q. J. Roy. Meteor. Soc., 133, 109–128, doi:10.1002/qj.143, 2007. 12875, 12879, 12889

Buehler, S. A., Defer, E., Evans, F., Eliasson, S., Mendrok, J., Eriksson, P., Lee, C., Jiménez, C., Prigent, C., Crewell, S., Kasai, Y., Bennartz, R., and Gasiewski, A. J.: Observing ice clouds in the submillimeter spectral range: the CloudIce mission proposal for ESA's Earth Explorer 8, Atmos. Meas. Tech., 5, 1529–1549, doi:10.5194/amt-5-1529-2012, 2012. 12879

Cotton, R., Field, P., Ulanowski, Z., Kaye, P. H., Hirst, E., Greenaway, R., Crawford, I., Crosier, J., and Dorsey, J.: The effective density of small ice particles obtained from in situ aircraft observations of mid-latitude cirrus, Q. J. Roy. Meteor. Soc., 139, 1923–1934, 2013. 12895

Davis, C. P., Wu, D. L., Emde, C., Jiang, J. H., Cofield, R. E., and Harwood, R. S.: Cirrus Induced Polarization in 122 GHz Aura Microwave Limb Sounder radiances, Geophys. Res. Lett., 32, L14806, doi:10.1029/2005GL022681, 2005. 12875

Debye, P.: Polar Molecules, The Chemical Catalog Company, Inc., New York, 1929. 12882

Doherty, A., Sreerekha, T., O'Keeffe, U., and English, S.: Ice hydrometeor microphysical assumptions in radiative transfer models at AMSU-B frequencies, Q. J. Roy. Meteor. Soc., 133, 1205–1212, 2007. 12877

Draine, B. T. and Flatau, P. J.: Discrete-dipole approximation for scattering calculations, J. Optical Soc. Am., 11, 1491–1499, 1994. 12877

Draine, B. T. and Flatau, P. J.: User Guide for the Discrete Dipole Approximation Code DDSCAT (Version 5a10), arXiv preprint astro-ph/0008151, 2000. 12884

Emde, C., Buehler, S. A., Davis, C., Eriksson, P., Sreerekha, T. R., and Teichmann, C.: A polarized discrete ordinate scattering model for simulations of limb and nadir long-

AMTD
7, 12873–12927, 2014

wave measurements in 1D/3D spherical atmospheres, J. Geophys. Res., 109, D24207, doi:10.1029/2004JD005140, 2004. 12895
Eriksson, P., Buehler, S. A., Davis, C. P., Emde, C., and Lemke, O.: ARTS, the atmospheric radiative transfer simulator, Version 2, J. Quant. Spectrosc. Ra., 112, 1551–1558, doi:10.1016/j.jqsrt.2011.03.001, 2011a. 12895
Eriksson, P., Rydberg, B., and Buehler, S. A.: On cloud ice induced absorption and polarisation effects in microwave limb sounding, Atmos. Meas. Tech., 4, 1305–1318, doi:10.5194/amt-4-1305-2011, 2011b. 12875, 12890
Evans, K. F. and Stephens, G. L.: Microwave radiative transfer through clouds composed of realistically shaped ice crystals, Part II. Remote sensing of ice clouds, J. Atmos. Sci., 52, 2058–2072, 1995a. 12875, 12879
Evans, K. F. and Stephens, G. L.: Microwave radiative transfer through clouds composed of realistically shaped ice crystals, Part I: single scattering properties, J. Atmos. Sci., 52, 2041–2057, 1995b. 12890
Evans, K. F., Wang, J. R., O'C Starr, D., Heymsfield, G., Li, L., Tian, L., Lawson, R. P., Heymsfield, A. J., and Bansemer, A.: Ice hydrometeor profile retrieval algorithm for high-frequency microwave radiometers: application to the CoSSIR instrument during TC4, Atmos. Meas. Tech., 5, 2277–2306, doi:10.5194/amt-5-2277-2012, 2012. 12877, 12879
Field, P. R., Heymsfield, A. J., and Bansemer, A.: Snow size distribution parameterization for midlatitude and tropical ice clouds, J. Atmos. Sci., 64, 4346–4365, 2007. 12897, 12898, 12900, 12925, 12926
Galligani, V. S., Prigent, C., Defer, E., Jiménez, C., and Eriksson, P.: The impact of the melting layer on the passive microwave cloud scattering signal observed from satellites: a study using TRMM microwave passive and active measurements, J. Geophys. Res., 118, 5667–5678, doi:10.1002/jgrd.50431, 2013. 12891
Garnett, J. M.: Colours in metal glasses, in metallic films, and in metallic solutions, II, Philos. T. R. Soc. Lond., 237–288, 1906. 12882
Geer, A. J. and Baordo, F.: Improved scattering radiative transfer for frozen hydrometeors at microwave frequencies, Atmos. Meas. Tech., 7, 1839–1860, doi:10.5194/amt-7-1839-2014, 2014. 12877, 12878, 12879, 12897, 12898, 12899, 12900, 12901, 12905, 12906
Gong, J. and Wu, D. L.: CloudSat-constrained cloud ice water path and cloud top height retrievals from MHS 157 and 183.3 GHz radiances, Atmos. Meas. Tech., 7, 1873–1890, doi:10.5194/amt-7-1873-2014, 2014. 12876

AMTD
7, 12873–12927, 2014

Hall, M. P., Goddard, J. W., and Cherry, S. M.: Identification of hydrometeors and other targets by dual-polarization radar, Radio Sci., 19, 132–140, 1984. 12875

Heymsfield, A. and McFarquhar, G.: Mid-latitude and tropical cirrus: Microphysical properties, Cirrus, 78–101, 2002. 12876

Hogan, R. J., Francis, P., Flentje, H., Illingworth, A., Quante, M., and Pelon, J.: Characteristics of mixed-phase clouds, I: lidar, radar and aircraft observations from CLARE'98, J. Molec. Struct., 129, 2089–2116, 2003. 12875

Hogan, R. J., Tian, L., Brown, P. R., Westbrook, C. D., Heymsfield, A. J., and Eastment, J. D.: Radar scattering from ice aggregates using the horizontally aligned oblate spheroid approximation, J. Appl. Meteorol. Clim., 51, 655–671, doi:10.1175/JAMC-D-11-074.1, 2012. 12876, 12893, 12895, 12921

Hong, G.: Parameterization of scattering and absorption properties of nonspherical ice crystals at microwave frequencies, J. Geophys. Res., 112, D11208, doi:10.1029/2006JD008364, 2007. 12886

Hong, G., Yang, P., Baum, B. A., Heymsfield, A. J., Weng, F., Liu, Q., Heygster, G., and Buehler, S. A.: Scattering database in the millimeter and submillimeter wave range of 100-1000 GHz for nonspherical ice particles, J. Geophys. Res., 114, D06201, doi:10.1029/2008JD010451, 2009. 12884, 12886, 12903, 12904, 12914, 12917, 12926

Hufford, G.: A model for the complex permittivity of ice at frequencies below 1 THz, Int. J. Infrared Milli., 12, 677–683, 1991. 12880, 12915

Jiang, J. H. and Wu, D. L.: Ice and water permittivities for millimeter and sub-millimeter remote sensing applications, Atmos. Sci. Lett., 5, 146–151, doi:10.1002/asl.77, 2004. 12880, 12915

Jiménez, C., Buehler, S. A., Rydberg, B., Eriksson, P., and Evans, K. F.: Performance simulations for a submillimetre wave cloud ice satellite instrument, Q. J. Roy. Meteor. Soc., 133, 129–149, doi:10.1002/qj.134, 2007. 12875

Johnson, B. T., Petty, G. W., and Skofronick-Jackson, G.: Microwave properties of ice-phase hydrometeors for radar and radiometers: Sensitivity to model assumptions, J. Appl. Meteorol. Clim., 51, 2152–2171, 2012. 12883

Kahnert, M., Sandvik, A. D., Biryulina, M., Stamnes, J. J., and Stamnes, K.: Impact of ice particle shape on short-wave radiative forcing: a case study for an arctic ice cloud, J. Quant. Spectrosc. Ra., 109, 1196–1218, 2008. 12889

AMTD
7, 12873–12927, 2014

Kim, M.-J.: Single scattering parameters of randomly oriented snow particles at microwave frequencies, J. Geophys. Res., 111, D14201, doi:10.1029/2005JD006892, 2006. 12877, 12889, 12904

Kulie, M. S., Bennartz, R., Greenwald, T. J., Chen, Y., and Weng, F.: Uncertainties in microwave properties of frozen precipitation: implications for remote sensing and data assimilation, J. Atmos. Sci., 67, 3471–3487, 2010. 12877, 12878, 12879

Liao, L., Meneghini, R., Nowell, H. K., and Liu, G.: Scattering computations of snow aggregates from simple geometrical particle models, IEEE J. Sel. Top. Appl., 6, 1409–1417, 2013. 12877, 12888, 12891, 12892

Liebe, H. J., Hufford, G. A., and Cotton, M. G.: Propagation modeling of moist air and suspended water/ice particles at frequencies below 1000 GHz, in: AGARD 52nd Specialists' Meeting of the Electromagnetic Wave Propagation Panel, 1–10 March, Palma de Mallorca, Spain, 1993. 12880

Liu, G.: Approximation of single scattering properties of ice and snow particles for high microwave frequencies, J. Atmos. Sci., 61, 2441–2456, 2004. 12877, 12889, 12894

Liu, G.: A database of microwave single-scattering properties for nonspherical ice particles, B. Am. Meteorol. Soc., 89, 1563, doi:10.1175/2008BAMS2486.1, 2008. 12877, 12884, 12903, 12904, 12914, 12917

Liu, Q., Xue, Y., and Li, C.: Sensor-based clear and cloud radiance calculations in the community radiative transfer model, Appl. Optics, 52, 4981–4990, 2013. 12876

Mätzler, C.: Thermal microwave radiation: applications for remote sensing, IET electromagnetic waves series, Institution of Engineering and Technology, 52, ISBN 9780863415739, 2006. 12881, 12885, 12904, 12915, 12917

McFarquhar, G. M. and Heymsfield, A. J.: Parameterization of tropical cirrus ice crystal size distribution and implications for radiative transfer: results from CEPEX, J. Atmos. Sci., 54, 2187–2200, 1997. 12901, 12925, 12926

Meirold-Mautner, I., Prigent, C., Defer, E., Pardo, J. R., Chaboureau, J.-P., Pinty, J.-P., Mech, M., and Crewell, S.: Radiative transfer simulations using mesoscale cloud model outputs: comparisons with passive microwave and infrared satellite observations for midlatitudes, J. Atmos. Sci., 64, 1550–1568, 2007. 12877

Millán, L., Read, W., Kasai, Y., Lambert, A., Livesey, N., Mendrok, J., Sagawa, H., Sano, T., Shiotani, M., and Wu, D. L.: SMILES ice cloud products, J. Geophys. Res., 118, 6468–6477, doi:10.1002/jgrd.50322, 2013. 12876, 12879

AMTD
7, 12873–12927, 2014

Mishchenko, M. I., Travis, L. D., and Mackowski, D. W.: T-matrix computation of light scattering by nonspherical particles: a review, J. Quant. Spectrosc. Ra., 55, 535–575, doi:10.1016/0022-4073(96)00002-7, 1996. 12876

Mishima, O., Klug, D. D., and Whalley, E.: The far-infrared spectrum of ice Ih in the range 8–25 cm^{-1}, sound waves and difference bands, with application to Saturn's rings, J. Comp. Phys., 78, 6399–6404, doi:10.1063/1.444700, 1983. 12880

Nowell, H., Liu, G., and Honeyager, R.: Modeling the microwave single-scattering properties of aggregate snowflakes, J. Geophys. Res., 118, 7873–7885, doi:10.1002/jgrd.50620, 2013. 12877, 12884, 12885, 12888, 12903, 12904, 12914, 12917

Petty, G. W. and Huang, W.: Microwave backscatter and extinction by soft ice spheres and complex snow aggregates, J. Atmos. Sci., 67, 769–787, 2010. 12884

Rydberg, B., Eriksson, P., Buehler, S. A., and Murtagh, D. P.: Non-Gaussian Bayesian retrieval of tropical upper tropospheric cloud ice and water vapour from Odin-SMR measurements, Atmos. Meas. Tech., 2, 621–637, doi:10.5194/amt-2-621-2009, 2009. 12876, 12879

Schmitt, C. G. and Heymsfield, A. J.: Observational quantification of the separation of simple and complex atmospheric ice particles, Geophys. Res. Lett., 41, 1301–1307, 2014. 12893

Sihvola, A.: Mixing rules with complex dielectric coefficients, Journal of Subsurface Sensing Technologies and Applications, 1, 393, doi:10.1023/A:1026511515005, 2000. 12882

Skofronick-Jackson, G. M., Gasiewski, A. J., and Wang, J. R.: Influence of microphysical cloud parameterizations on microwave brightness temperatures, IEEE Geosci. Remote S., 40, 187–196, 2002. 12877

Tyynelä, J. and Chandrasekar, V.: Characterizing falling snow using multifrequency dual-polarization measurements, J. Geophys. Res., 119, 8268–8283, doi:10.1002/2013JD021369, 2014. 12884

Warren, S.: Optical constants of ice from the ultraviolet to the microwave, Appl. Optics, 23, 1206–1225, doi:10.1364/AO.23.001206, 1984. 12880, 12882, 12886, 12904, 12915

Warren, S. G. and Brandt, R. E.: Optical constants of ice from the ultraviolet to the microwave: A revised compilation, J. Geophys. Res., 113, D14220, doi:10.1029/2007JD009744, 2008. 12881, 12904, 12915

Wilson, D. R. and Ballard, S. P.: A microphysically based precipitation scheme for the UK Meteorological Office Unified Model, Q. J. Roy. Meteor. Soc., 125, 1607–1636, 1999. 12900

AMTD
7, 12873–12927, 2014

Wu, D. L., Jiang, J. H., Read, W. G., Austin, R. T., Davis, C. P., Lambert, A., Stephens, G. L., Vane, D. G., and Waters, J. W.: Validation of the Aura MLS cloud ice water content measurements, J. Geophys. Res., 113, D15S10, doi:10.1029/2007JD008931, 2008. 12876, 12879

Wu, D. L., Lambert, A., Read, W. G., Eriksson, P., and Gong, J.: MLS and CALIOP cloud ice measurements in the upper troposphere: A constraint from microwave on cloud microphysics, J. Appl. Meteorol. Clim., 53, 157–165, doi:10.1175/JAMC-D-13-041.1, 2014. 12890

Zhang, C., Lee, K.-S., Zhang, X.-C., Wei, X., and Shen, Y.: Optical constants of ice Ih crystal at terahertz frequencies, Appl. Phys. Lett., 79, 491–493, doi:10.1063/1.1386401, 2001. 12880, 12915

Zhao, L. and Weng, F.: Retrieval of ice cloud parameters using the Advanced Microwave Sounding Unit, J. Appl. Meteorol., 41, 384–395, 2002. 12876

AMTD
7, 12873–12927, 2014

Table 1. Overview of considered DDA databases.

Database	Frequency range [GHz]	Temperatures [K]	Particle sizes [μm, max. dim.]	Particle shapes
Liu (2008)	3.0–340	233, 243, 253, 263 and 273	50–12 454	Columns, plates, rosettes, sector and dendrite snowflakes.
Nowell et al. (2013)	10.65–183.31	263	200–12 584	Three aggregate types, consisting of 200 and/or 400 μm 6-bullet rosettes.
Hong et al. (2009)	90–874	243	2–2000	Solid and hollow columns, plates, 6-bullet rosettes, droxtals and one type of aggregate.

AMTD
7, 12873–12927, 2014

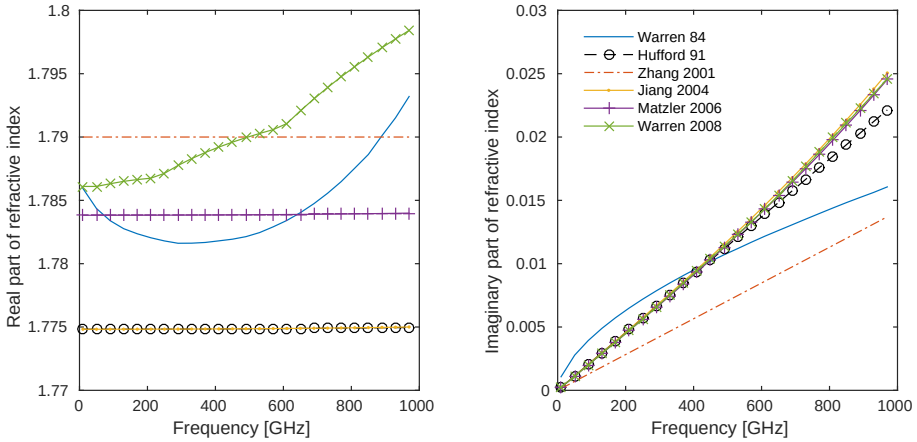

Figure 1. Real (left) and imaginary (right) part of the refractive index of pure ice, as a function of frequency, according to Warren (1984), Hufford (1991), Zhang et al. (2001), Jiang and Wu (2004); Mätzler et al. (2006) and Warren and Brandt (2008). The temperature is set to 266 K.

AMTD
7, 12873–12927, 2014

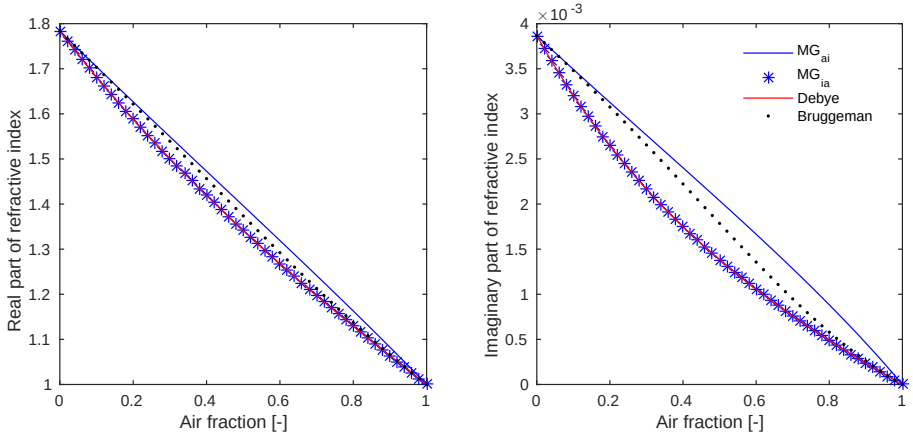

Figure 2. Real (left) and imaginary (right) part of the effective refractive index of a mixture of ice and air, as a function of air volume fraction according to some mixing rules. The refractive index of ice at 183 GHz and 263 K, $n_{ice} = 1.7831 + i0.0039$, was used, and the refractive index of air was set to $n_{air} = 1 + i0$.

AMTD
7, 12873–12927, 2014

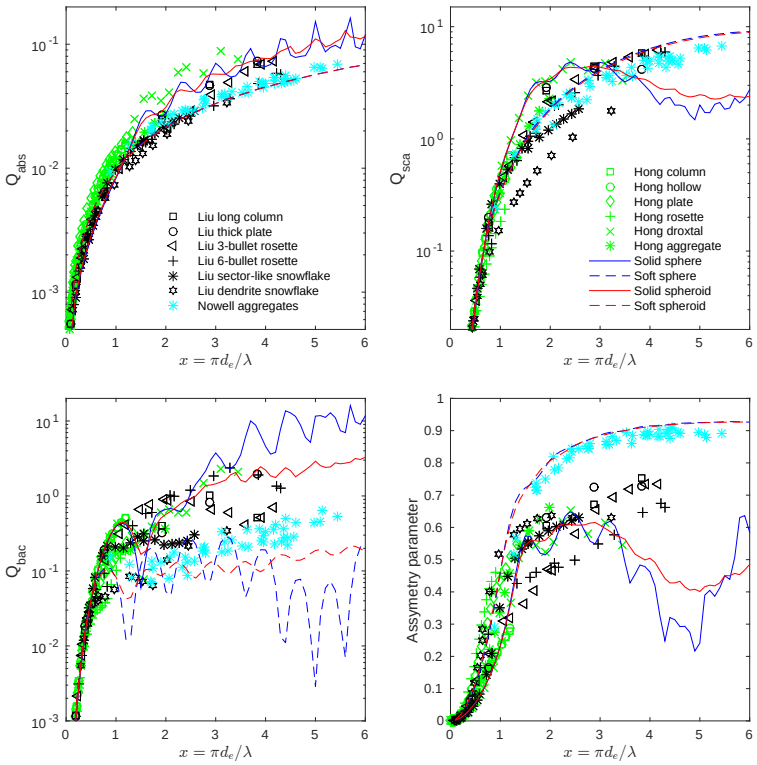

Figure 3. DDA-based single scattering properties at 183 GHz from the databases of Liu (2008); Nowell et al. (2013) and Hong et al. (2009). Absorption, scattering and back-scattering efficiencies (Eq. 10) and asymmetry parameter are displayed. The combined legends are valid for all panels. The figure includes also data of solid and soft spheres and spheroids, with refractive index following Mätzler et al. (2006). The soft particles have an air fraction of 0.75, with the effective refractive indices derived by the MG_{ai} mixing rule. The spheroids are oblate with an aspect ratio of 1.67. All results are valid for 183 GHz and 243 K, except Nowell et al. (2013) that are for 263 K.

AMTD
7, 12873–12927, 2014

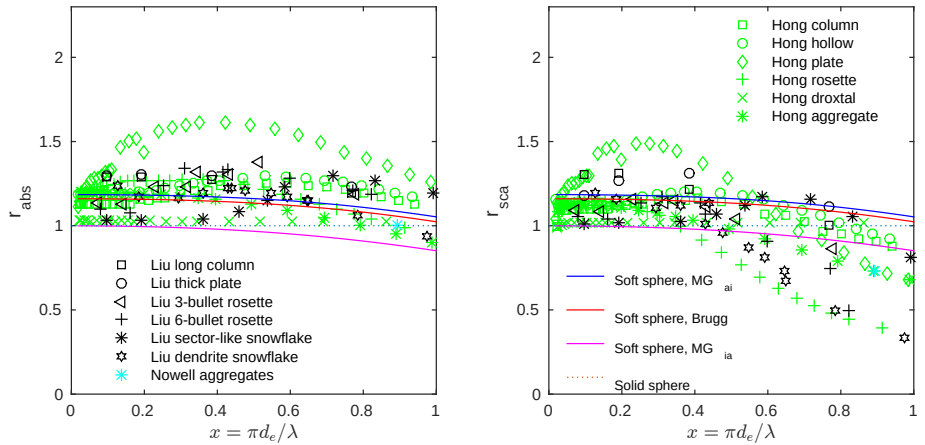

Figure 4. Absorption (left) and scattering (right) cross-sections of DDA data and soft spheres at 183 GHz. The cross-sections are reported as the ratio to the corresponding cross-section of the equivalent mass sphere, with the same refractive index as used for the preparation of the DDA data. That is, the dotted straight line at $r = 1$ represents solid ice spheres. Database source and particle shapes of the DDA data are found in figure legends (same as in Fig. 3). The soft spheres have an air fraction of 0.25, where results for three different mixing rules (MG_{ia}, Bruggeman and MG_{ia}) are included (solid lines).

AMTD
7, 12873–12927, 2014

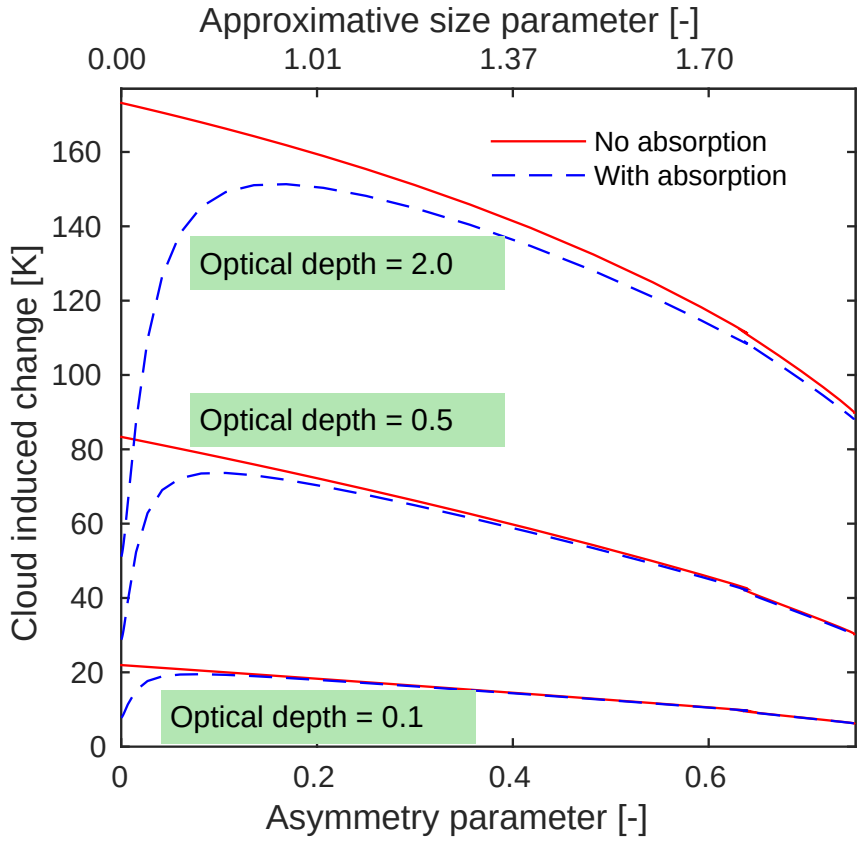

Figure 5. Test of importance of absorption and asymmetry parameter for passive microwave radiative transfer. The brightness temperature deviation from simulations with no cloud layer is reported. The stated optical depths refer to the zenith extinction of the cloud layer. For solid lines, the imaginary part of the refractive index was set to zero, resulting in no cloud particle absorption. The simulations are described further in the text.

AMTD
7, 12873–12927, 2014

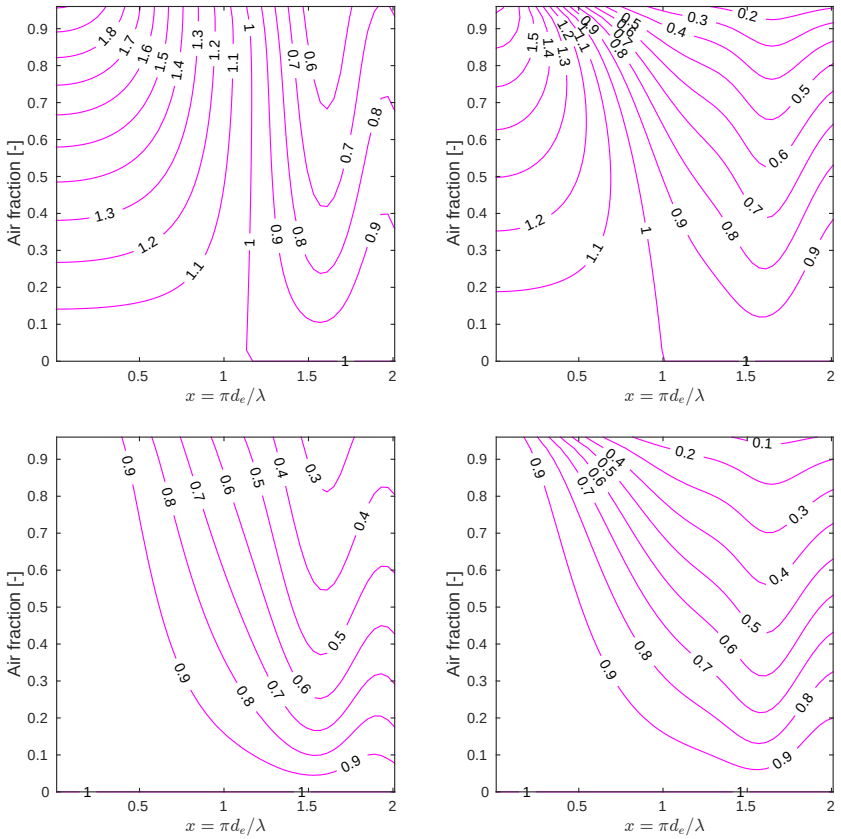

Figure 6. Absorption (left) and scattering (right) cross-sections of soft spheres (183 GHz and 243 K), normalised by the equivalent mass ice sphere absorption or scattering cross-section as in Fig. 4, as a function of size parameter and air fraction. The two top panels are calculated using the MG_{ai} (air in ice) mixing rule, while the two lower panels are calculated using the MG_{ia} (ice in air) mixing rule.

AMTD
7, 12873–12927, 2014

Ice hydrometeor microwave optical properties

P. Eriksson et al.

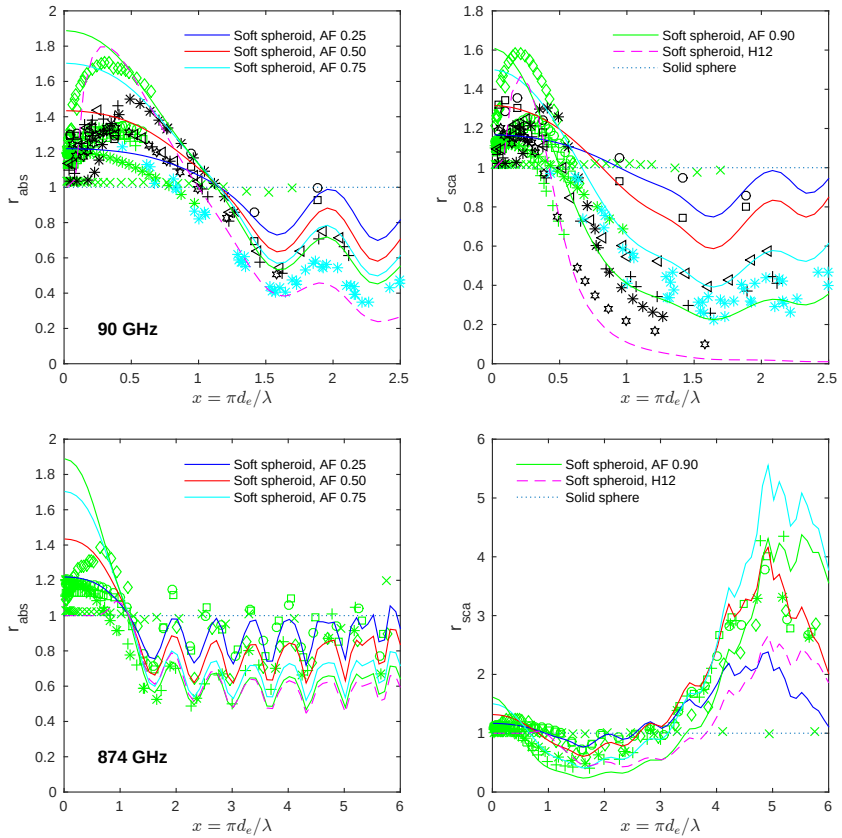

Figure 7. Normalised absorption (left) and scattering (right). The top row includes 90 GHz Hong/Liu and 89 GHz Nowell data, while the bottom row covers 874 GHz. The soft spheroids have either a fixed air fraction (AF) or follow Hogan et al. (2012), denotes as H12. Normalisation and plotting symbols used for DDA data as in Fig. 4.

AMTD
7, 12873–12927, 2014

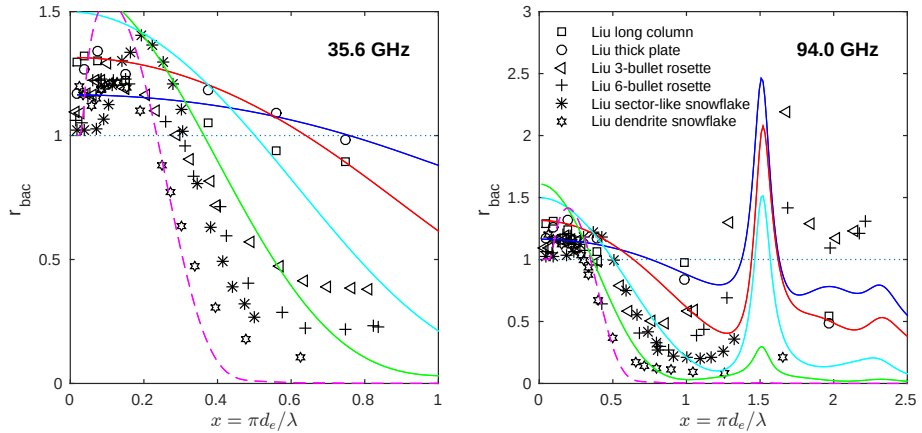

Figure 8. Normalised back-scattering of the Liu particles at two frequencies. As in Figs. 4 and 7, the normalisation is performed with respect to the back-scattering cross-section of the solid sphere having the same mass. For 94 GHz and $x \approx 1.5$ some data points have a ratio above 3, partly due to a minimum of the solid sphere back-scattering at that size parameter. Solid and dotted lines are the same as in Fig. 7.

AMTD
7, 12873–12927, 2014

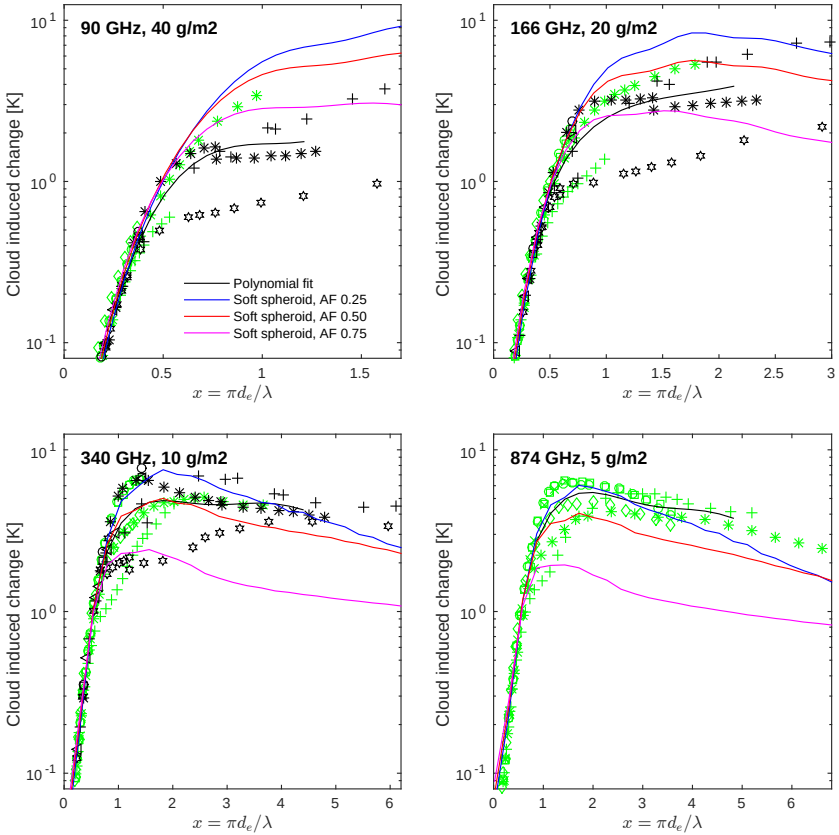

Figure 9. Radiative transfer simulations at different frequencies. General conditions as in Fig. 5, i.e. a 2 km thick cloud layer at 10 km is simulated. A single particle type is included in each simulation where the number density was adjusted to obtain the stated ice water paths. The black solid line is a high-order polynomial fit of the DDA-based results, while other lines are results for soft spheroids with constant air fraction (AF).

AMTD
7, 12873–12927, 2014

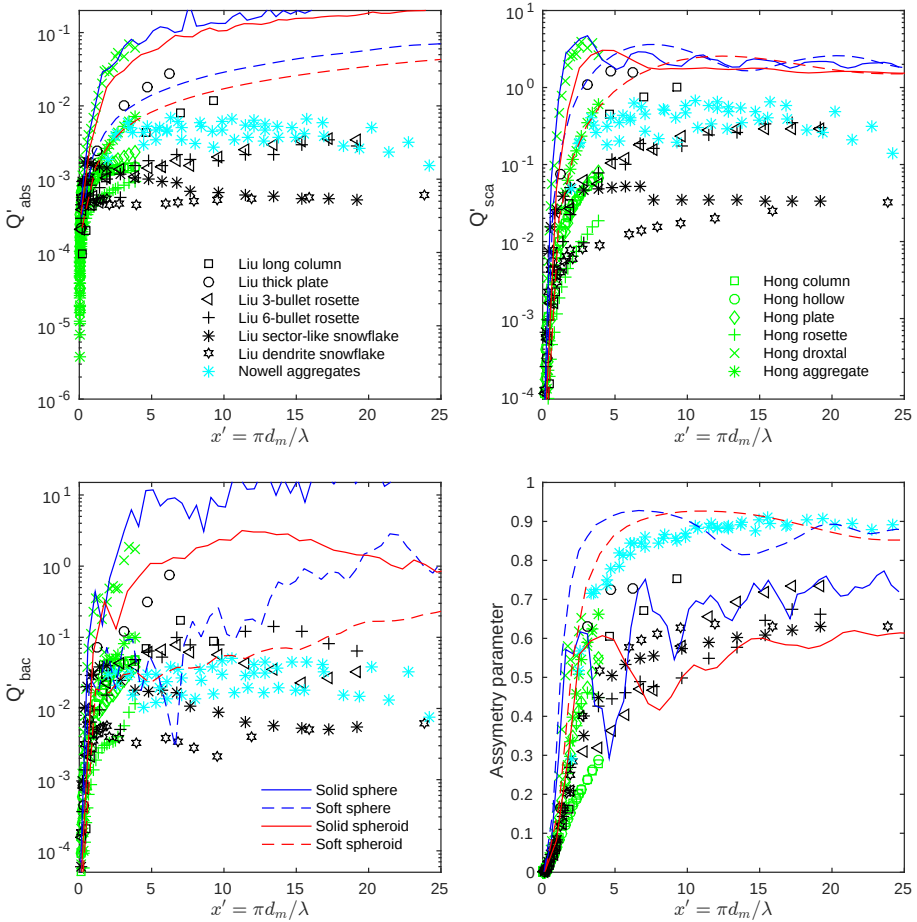

Figure 10. As Fig. 3, but using the maximum dimension (d_m) as characteristic size. That is, the size parameter is here defined as $x' = \pi d_m/\lambda$ and absorption and scattering efficiencies are defined as $Q' = (4\sigma)/(\pi d_m^2)$. As in Fig. 3, the frequency is 183 GHz.

AMTD
7, 12873–12927, 2014

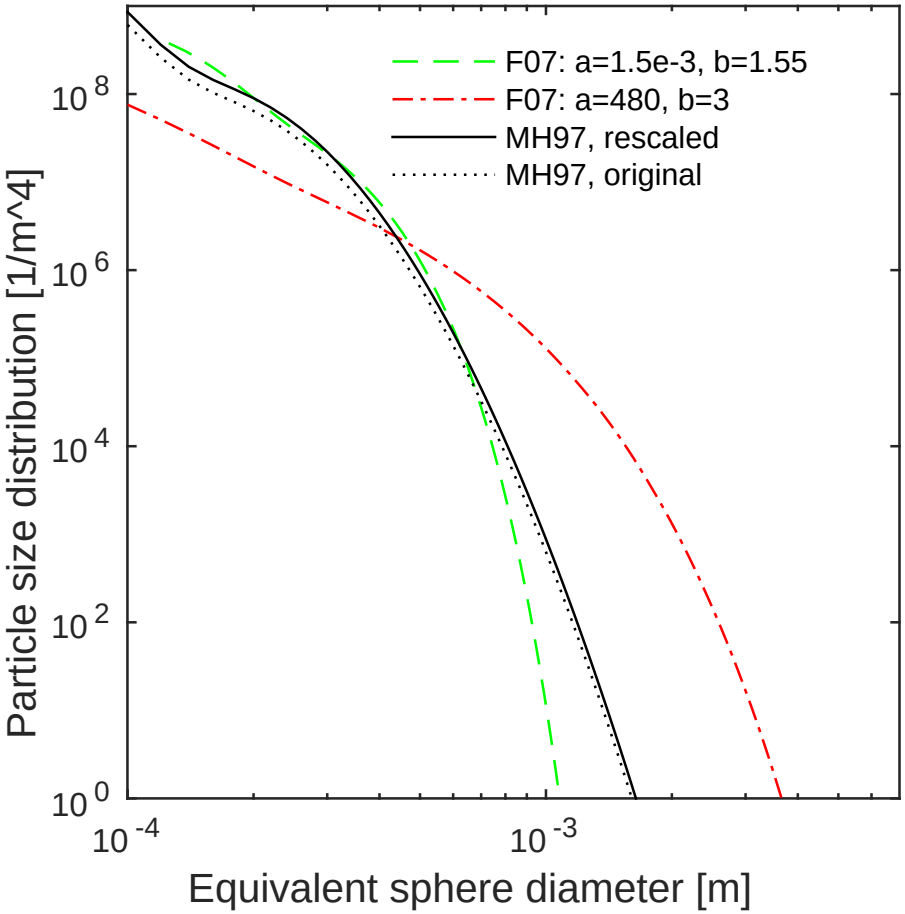

Figure 11. Ice particle size distributions for 0.1 g m^{-3}, according to Field et al. (2007, F07) and McFarquhar and Heymsfield (1997, MH97). The F07 PSD is converted from d_m to d_e for two combinations of a and b (Eq. 11).

AMTD
7, 12873–12927, 2014

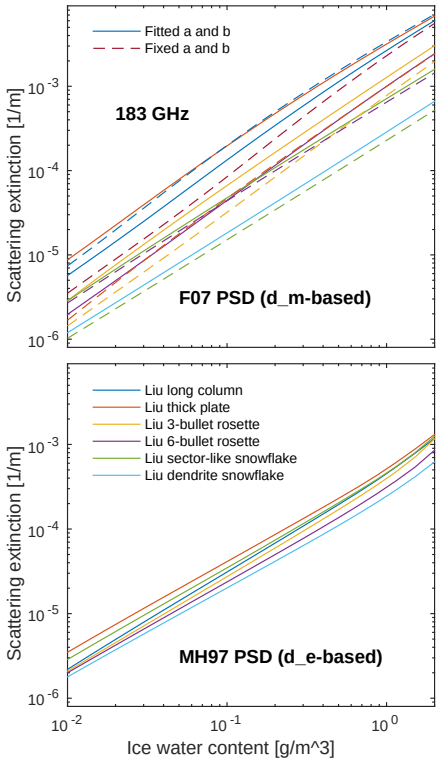

Figure 12. Scattering extinction as a function of ice water content at 183 GHz, for some of the particles of the Hong et al. (2009) DDA database. The particle size distribution applied in the upper and lower panels is F07 (Field et al., 2007) and MH97 (McFarquhar and Heymsfield, 1997), respectively. Dashed lines in the upper panel show results for the F07 distribution with fixed $a = 0.069$ and $b = 2$.

AMTD
7, 12873–12927, 2014

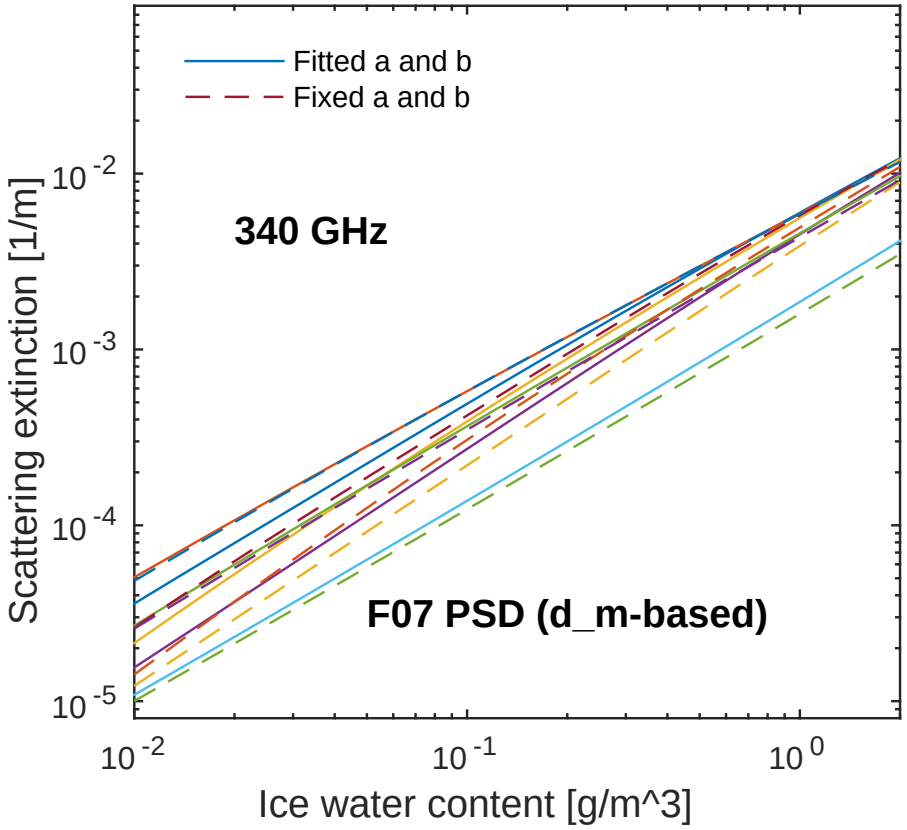

Figure 13. As Fig. 12, but for 340 GHz. The results for MH97 are not shown as they show the same general pattern as in Fig. 12 (just shifted in mean level in same way as the results for F07).

AMTD
7, 12873–12927, 2014